ABSTRACT

Nanoparticles are one of the fundamental building blocks of nanotechnology. Their physico-chemical properties like melting point, chemical reactivity etc. change rapidly with particle size in the nano-scale range. Currently, development of synthesis protocols for optimizing particle size and its distribution to exploit their size-dependent properties is a formidable research challenge. The main objective of this work is to develop a protocol, which is reproducible and repeatable, to synthesize gold nanoparticles using microemulsions. Microemulsions (reverse micelles) are self-assembled aggregates of surfactant layers between aqueous and organic phases. Microemulsion based nanoparticle synthesis can aid the precise control of particle size and its distribution by varying the above parameters in conjunction with processing conditions either simultaneously or independently. Typically, nanoparticles are prepared by mixing two microemulsion solutions containing the precursor and reducing agent respectively.

Nanoparticle size and polydispersity were characterized using Dynamic light scattering (DLS), UV-visible spectroscopy (UV-vis) and Transmission electron microscopy (TEM). Water/AOT/Brij 30/isooctane was used as the templating system. Gold nanoparticles were formed in a redox reaction by mixing freshly prepared reverse micellar solutions containing gold chloride and hydrazine hydrate. Based on preliminary UV-vis results, it has been found that the amount of hydrazine has to be twelve times more than the stochiometric requirements to completely reduce gold chloride, due to some side reaction between AOT and hydrazine, resulting in imine formation.

The area under the Surface Plasmon Resonance (SPR) peak in the UV-vis spectra has been used to characterize the stability of the particles in solution. It was also established that sonication helps in reducing the polydispersity of the droplet, with the time of sonication being a critical parameter. The presence of co-surfactants like Brij 30 or Brij 52 helps in increasing the efficiency of micelle fusion compared to the water-AOT-isooctane system. In view of maintaining a reproducible mixing strategy, a standard four-blade Rushton impeller with baffles (all parts made of Teflon®) was designed and fabricated. In this study, the effect of parameters such as rate of addition of

reducing agent, and reactant concentration on nanoparticle size and polydispersity were investigated. The particle size and polydispersity was found to increase with decrease in addition rate. With temperature, there was no drastic effect on particle size. However, the yield of nanoparticles gets drastically affected with increase in temperature and decrease in addition rate. The onset of pink color upon addition of reducing agent to gold chloride micellar solution is found to be a probable indicator of start of growth phase.

TABLE OF CONTENTS

LIST OF TABLES

Table **Page**

LIST OF FIGURES

Figure **Page**

Chapter 1

Introduction

Nanoscience refers to the study of the fundamental principles of molecules and structures with at least one dimension between 1 to 100 nanometers, while nanotechnology refers to the application of these structures to form useful devices [1]. Nanotechnology involves the capability to synthesize, characterize and control such artificial structures [2]. Nanoparticles are one of the fundamental building blocks of nanotechnology having all three dimensions in the nanoscale regime. Nanoparticles exhibit behavior which is intermediate between bulk solid and molecular system. The scientific study of metal nanoparticles has generated a lot of interest from the time of Michael Faraday's pioneering experiments [2].

1.1 Nanoparticles and their applications

Nanoparticles of noble metals namely gold, silver and copper have attracted the largest share of scientific interest, and in particular, gold nanoparticles have been studied extensively in literature and are being used for technological applications. Gold nanoparticles show remarkable catalytic activity while their bulk counterpart is inert in nature. The increase in reactivity with decrease in particle size can be attributed to the increasing proportion of surface atoms. Magnetic nanoparticles are attracting interest due to their technological importance. Magnets are being used in data storage devices, power transformations, motors, electronics etc. With miniaturization, magnetic properties like coercive force, anisotropy etc., can be precisely controlled. For example, the coercive force, which is the force required for inverting a magnetic field decreases with a decrease in particle size [3]. In particular, Fe-Pt nanoparticles are attractive candidates for applications involving memory devices because of their large uniaxial magnetic anisotropy energy (~ 6.6 MJ m^{-3}) [4].

1.2 Nanoparticle synthesis: An overview

The size and shape of nanoparticles have received much attention in recent years, due to their strong effects on the physical and chemical properties of nanoparticles [5]. Size dependent properties of nanoparticles can be exploited in many applications ranging from electronics to biomedical industry. In general, the synthesis routes can be broadly classified into two categories namely gas phase and solution phase synthesis.

Gas phase processes [6] involve the generation of metal atoms leading to homogeneous nucleation and subsequent condensation and coagulation of nanoparticles. Gas phase processes can be classified into inert gas condensation, plasma sputtering, pulsed laser ablation, spark discharge generation etc., depending on the source for generating nuclei**.** Absence of hazardous chemicals like borohydride, hydrazine etc. and good control over the mean particle size and their distribution are few advantages of gas phase processes. However, energy expenditure, use of sophisticated equipment etc., are major disadvantages of these processes. Especially, in inert gas condensation technique, the failure of evaporation source, inhomogeneous temperature distribution, problems related to gas flow like vortex formation greatly affect the quality of nanoparticles obtained [6].

Solution phase syntheses involve reduction of metal precursor salts to metal atoms using chemical reaction. Various classifications like sonochemical, sonomechanical, polyol, microemulsions routes can be made depending on the method employed for the chemical reduction of the precursor. Nanoparticle synthesis using microemulsions has attracted technological interest, as it offers several engineering parameters to control the particle size and its distribution, and also the synthesis can be carried out at or near room temperature.

1.3 Project objectives

Metal nanoparticles are relatively easy to synthesize at the lab-scale by either chemical or aerosol techniques; the barriers in manufacturing these particles are associated with limitations in scaling up their volume. To overcome these limitations, predictive control of particle size and its distribution is needed. The synthesis of nanoparticles using microemulsions is a potential option for manufacture of

nanoparticles. This project is a follow-up on the work initiated earlier by D. Surya [7] and C. Dupeu [8]. They synthesized gold nanoparticles following a recipe reported in the literature [9]. The reduction has been reported to occur by the following reaction:

$$4HAuCl_4 + 3N_2H_5OH \rightarrow 4Au + 16HCl + 3N_2 + 3H_2O \quad (1.1)$$

Their results showed an interesting trend of change in particle size with the change in rate of addition of reducing agent. However, the results were not repeatable or reproducible. It was also reported that aging of reactants (both in reverse micelles and in aqueous solution) is necessary for synthesizing nanoparticles. An objective of this work is to develop a synthesis protocol for preparing stable gold nanoparticles using microemulsions that is reproducible and repeatable. Also, the protocol has to be used as template for synthesizing other nanoparticles like Ag, Fe-Pt etc. This entails a careful study using Dynamic Light Scattering (DLS) to characterize the size and polydispersity of reverse micelles formed under different preparatory conditions. A major goal of this project is a parametric study of the effect of temperature and reagent addition rate on particle size and its distribution.

This report has been organized in the following way. In chapter 2, an overview on microemulsions is presented along with a literature review on nanoparticle synthesis using microemulsions. A brief introduction on experimental set-up along with the sample characterization techniques employed in this study are discussed in chapter 3. In chapter 4, preliminary studies carried out for synthesizing stable gold nanoparticles is presented. Chapter 5 discusses the study using DLS characterization of reverse micelles. Chapter 6 focuses on the scaling up of the system along with the parametric study of the effect of temperature and hydrazine addition rate on particle size and distribution. Chapter 7 summarizes the major contributions of this work followed by recommendations for further work.

1.4 References

[1]. M. Ratner and D. Ratner, 'Nanotechnology, A Gentle Introduction to the Next big Idea', Pearson Publications, 2005.

[2]. G. Schmid, 'Nanoparticle, From Theory to Application' Wiley–VCH Verlag Gmbh and Co., 2004.

[3]. Q. Chen and Z. J. Zhang, 'Size-dependent superparamagnetic properties of $MgFe_2O_4$ spinel ferrite nanocrystallites', Applied Physics Letters, 73, (23), 1998, pp. 3156-3158.

[4]. Q. Y. Yan, T. Kim, A. Purkayastha, Y. Xu, M. Shima, R. J. Gambino and G. Ramanath 'Magentic properties of Sb-doped FePt nanoparticles', Journal of Applied Physics, 99, 2006, pp. 08N7091-08N7093.

[5]. X. Ren, D. Chen, and F. Tang, 'Shape-controlled synthesis of copper colloids with a simple chemical route', Journal of Physical Chemistry B, 109, 2005, pp.15803-15807.

[6]. C. Baker, A. Pradhan and I. Shah, 'Metal nanoparticles', Encyclopedia of Nanoscience and Nanotechnology', Vol.5, Edited by H. S. Nalwa, 2004, pp. 449-473.

[7]. D. Surya, 'Synthesis and characterization of gold nanoparticles', Master of Engineering report, Indian Institute of Science, 2006**.**

[8]. C. Dupeu, 'Size control of gold nanoparticles synthesized in mixed reverse micelles', Project report on Indian Institute of Science, 2005.

[9] C. L. Chiang, 'Controlled growth of gold nanoparticles in AOT/$C_{12}E_4$/Isooctane mixed reverse micelles', Journal of Colloid and Interface Science, 239, 2001, pp.334–341.

Chapter 2

Microemulsions: An overview

The objective of this work is to synthesize nanoparticles using microemulsions. In general, microemulsions are self-assembled aggregates of amphipiles located between aqueous and organic phase. This self-assembly can exist in different shapes ranging from lamellar to spherical depending on the conditions like surfactant concentration, temperature etc [1]. This entails a careful study on microemulsions and factors affecting their shape and size. In literature, microemulsions are also called as swollen micelles, solubilizing micelles and micellar solutions [1]. The transparent emulsions that scatter light were first called "microemulsions" by Schulman et al. in 1959. Microemulsions have droplet diameters in the range of 10 to 200 nanometers [1]. A commonly employed amphiphile is Sodium 2-ethyl sulfosuccinate (Aerosol OT or AOT). In this chapter, a brief overview on microemulsions is presented along with literature review on nanoparticle synthesis using microemulsions. Also, the advantages and disadvantages related with employing AOT as the surfactant is discussed along with the role of co-surfactant.

2.1 Microemulsions

Amphiphiles (or surfactants) are molecules that possess both polar and non-polar groups. In aqueous (organic) solutions, surfactant dissolves and exists as monomer. However, as the concentration of surfactant exceeds critical micellar concentration (CMC), the molecules self-assemble to form aggregates called micelles (reverse micelles) [2]. In reverse micelle systems, the presence of water leads to larger surfactant aggregates called microemulsions or water droplets. The size of the reverse micelle is linearly dependent on the water content [2]. The properties of water in the reverse micelle depend on the molar ratio of water to surfactant. At higher ratio, the properties of water approach that of pure water [1]. A cubic and hexagonal phase is found in more concentrated mixtures. The surfactant in general can be anionic (e.g. Sodium

dodecylsulfate), cationic (e.g. Cetylpyridinium bromide), zwitterionic (e.g. Dipalmitoylphosphatidylcholine) or nonionic (e.g. Polyoxyethylene (4) lauryl ether, Brij 30). Sodium 2-ethyl sulfosuccinate, commonly called Aerosol OT or AOT is a common anionic surfactant that is used to form microemulsions. In general, cationic surfactants are more difficult to handle as they tend to adsorb on anionic surfaces (glass/quartz), while nonionic surfactants are more sensitive towards temperature [3].

2.1.1 Hydrophilic-Lipophilic balance (HLB)

The formation of o/w reverse micelles is strongly influenced by strong hydrophobic interactions (surfactant tail); while hydrophilic interactions (polar head group) drives w/o reverse micelles [4]. Depending on the hydrophilic-lipophilic balance (HLB), the system can exhibit either water in oil or oil in water microemulsions. From qualitative viewpoint, a change in the lipophilicity must be balanced by a corresponding change in the hydrophilicity, if the original interfacial behavior of surfactant has to be preserved. A slight alteration in the hydrophilicity or lipophilicity can affect the phase behavior drastically [4]. Lower HLB (4-7) results in w/o emulsions while higher HLB (9-20) results in o/w emulsions. In between w/o and o/w emulsions, different phase resembling sponge-like structure can exist [1].

2.1.2 Packing parameter

The geometry of the micellar aggregates can be predicted from the packing parameter of the surfactant molecules [4]. It is defined as $v/a_* l$ where "v" refers to lipophilic group volume, "a" refers to the area of the hydrophilic group and "l" refers to the maximum extended length of the surfactant molecule. The value of packing parameter is not solely affected by molecular structure, but also influenced by amount of water, organic phase and other amphiphilic molecules [4]. The volume of the cylinder with the cross-sectional area "a" and a length "l" equals "$a_* l$". If the packing parameter is less than 0.5, then the lipophilic group volume is less than the cylindrical volume. In this case, the molecules will be curved so as to enclose the lipophilic regions resulting in spherical aggregates. If the packing parameter lies between 0.5 and 1.0, then it will result in lesser curvature leading to cylindrical aggregate geometry. Alternatively, if the

packing parameter is greater than 1.0, the minimal curvature is expected, which will result in lamellar aggregate geometry [4].

2.2 Aerosol OT (AOT)

AOT is one of the most commonly employed surfactant in reverse micellar studies. The mean aggregation number (number of AOT molecules per reverse micelle) of AOT in n-octane, n-decane and n-dodecane are 30, 37 and 44 [5]. The CMC is reported to be of the order of a few mM [5]. In AOT/isooctane, the smallest aggregates have a hydrodynamic radius of 1.5 nm which is larger than the extended length of the surfactant molecule (1.1-1.2 nm) [5]. The presence of impurities in AOT can have drastic effects on the kinetics of reactions in microemulsions and to a lesser extent on the solubilization capacity. In general, there are two classes of impurities, one resulting from the manufacturing process of AOT and the other resulting during the formation of microemulsions [5]. Whether initially present or produced during the micellar formation, the micellar size and exchange rate can get affected. Hence, it is better to use high purity AOT or purify AOT before preparation of reverse micellar solutions in order to reduce error in reproducibility of the results. The rate of chemical reaction depend on parameters like water pool size, surfactant concentration etc., which can be easily tuned to effect a change in the system under study.

2.3 Percolation threshold

Reverse micelles are highly dynamic structures. Droplets collide, form transient aggregates and revert back to being isolated droplets. At low concentration of the dispersed phase, the system consists of identical spherical droplets while at higher concentrations, overlapping of droplets take place [6]. However, this depends on whether the interaction between droplets is attractive or repulsive. If the interactions are attractive, the duration of micelle collision increases, and transient clusters are formed. Usually, the cluster lifetimes are of the order of microseconds [6]. The overlapping of droplets results in exchange of solute. The exchange is generally achieved by either hopping of ions (or molecules) through interfaces or by transient opening of interfaces [7]. As the continuous phase of water in oil microemulsions is non-conducting, electrical

conduction needs contact of droplets, which is achieved by either hopping of transient merging of droplets. This condition can be quantitatively determined from the phenomenon called "percolation threshold" [7]. Percolation threshold is the point at which for a certain composition of dispersed phase (at constant temperature) or at certain temperature (at constant composition), there is a sharp increase in the conductivity of the solution, which can span two to three orders of magnitude [7]. This sharp increase can be attributed to the micelle clusters that allow charged material to be exchanged between them. Any external force which has an effect on micelle clustering will affect percolation process. Typically, the percolation process is affected by the presence of co-surfactants. More often than not, the co-surfactants employed with AOT are either alcohols or poly-(oxyethyl) alkyl ethers (C_iE_j). These two classes of co-surfactants have opposite effects on the percolation process. Also, it has been reported that the micellar clustering is made difficult by the presence of alcohols, while poly (oxyethy) alkyl ethers make clustering easier [7].

2.4 Nanoparticle synthesis using microemulsions

The synthesis of nanoparticles consists in mixing two microemulsions (having suitable reactants) to obtain desired particles. During the collision of droplets, the reactants get exchanged. For example, in the case of synthesis of metal nanoparticles, typical reactants are a reducing agent and a metal salt.

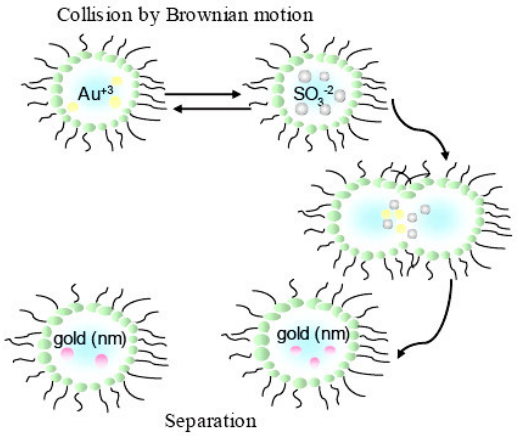

Fig. 2.1: Schematic representation of intermicellar exchange process [8]

A schematic representation of an intermicellar exchange process is shown in Figure 2.1. This exchange is so fast that the process is completed during initial mixing [6]. Then, the process of nucleation and growth takes place, which determines the final size of the particle and its distribution. Exchange of nuclei or particles is hindered as it requires huge change in the curvature of surfactant, which is not favored energetically.

Reverse micelles have been used to produce nanoparticles of pure metals like gold [9], copper [10], alloys like Fe-Pt [11], semiconductor materials like CdS, ZnS etc [12]. Pileni et al. have controlled the size and shape of copper nanoparticles with diameter ranging from 3 nm to 13 nm, using reverse micellar route [13]. Sato et al. have studied the mechanism of formation of CdS and ZnS nanoparticles by reverse micellar route [14]. They injected H_2S in the reverse micellar solution of $Cd(NO_3)_2$ to obtain CdS nanoparticles. They replaced $Cd(NO_3)_2$ with $Zn(NO_3)_2$ to obtain ZnS nanoparticles. They also found that the rate of injection can affect both nucleation and growth. Carpenter et al. synthesized Fe-Pt nanoparticles using microemulsions of iron and platinum salts [15]. The reverse micelles were formed using CTAB, 1-butanol (co-surfactant) and octane (oil phase). Sodium borohydride was used to reduce the metal salts, resulting in the formation of Fe-Pt nanoparticles. Gibot et al. have mixed $H_2PtCl_6 \cdot H_2O$ and $FeCl_2 \cdot H_2O$ with water along with hydrazine and a surfactant (CTAB) to form Fe-Pt nanoparticles [11].

2.5 Conclusions

This chapter gave an overview of parameters such as hydrophilic-lipophilic balance (HLB), packing parameter, and percolation threshold. These parameters help in deciding the right combination of surfactant and co-surfactant for preparing microemulsions. Here, the microemulsions are exploited for the synthesis of nanoparticles which will be discussed in the subsequent chapters. In this study, the mixed microemulsion consisting of water, sodium-bis-2(ethylhexyl) sulfosuccinate (AOT), polyoxyethlene-4-lauryl ether (Brij 30) and isooctane was used as the templating system. Gold nanoparticles were formed in a redox reaction by mixing freshly prepared reverse micellar solutions containing gold chloride ($HAuCl_4.3H_2O$) and hydrazine hydrate (N_2H_5OH) respectively.

2.6 References

[1]. L. M. Prince, 'Microemulsions: Theory and practice', Academic press, 1977, pp. 1-145.

[2]. M. P. Pileni, 'Water in oil colloidal droplets used as microreactors', Advances in Colloid and Interface Science, 46, 1993, pp. 139-163.

[3]. M. A. Michaels, 'Quantitative model for the prediction of hydrodynamic size of nonionic reverse micelles', Master of Science report, Virginia Commonwealth University, 2006.

[4]. R. G. Laughlin, 'The aqueous phase behavior of surfactants', Academic press, 1996, pp. 328-414.

[5]. T. K. De and A. Maitra, 'Solution behavior of Aerosol OT in nonpolar solvents', Advances in Colloid and Interface Science, 59, 1995, pp. 95-193.

[6]. I. Capek, 'Preparation of metal nanoparticles in water-in-oil (w/o) microemulsions', Advances in Colloid and Interface Science, 110, 2004, pp. 49-74.

[7]. L. M. M. Nazario, T. A. Hatton and J. P. S. G. Crespo, 'Nonionic co-surfactants in AOT reversed micelles: Effect on percolation, size, and solubilization site', Langmuir, 12, 1996, pp. 6326-6335.

[8]. A. P. H. Barros, 'Synthesis and agglomeration of gold nanoparticles in reverse micelles', Master of Science report, University of Puerto Rico, 2005.

[9]. C. L. Chiang, 'Controlled growth of gold nanoparticles in AOT/$C_{12}E_4$/Isooctane mixed reverse micelles', Journal of Colloid and Interface Science, 239, 2001, pp.334–341.

[10]. M. P. Pileni, 'Nanosized particles made in colloidal assemblies', Langmuir, 13, 1997, pp. 3266-3276.

[11]. P. Gibot, E. Tronc, C. Chaneac, J.P. Jolivet, D. Fiorani, A.M. Testa, '(Co,Fe)Pt nanoparticles by aqueous route; self-assembling, thermal and magnetic properties', Journal of Magnetism and Magnetic Materials, 290, 2005, pp 555–558.

[12]. T. Hirai, H. Sato, and I. Komasawa, 'Mechanism of formation of CdS and ZnS ultrafine particles in reverse micelles,' Industrial and Engineering Chemistry Research, 33, 1994, pp. 3262-3264.

[13]. C. Salzemann, I. Lisiecki, J. Urban, and M.P. Pileni, 'Anisotropic copper nanocrystals synthesized in a supersaturated medium: Nanocrystal growth', Langmuir, 20, 2004, pp. 11772-11777.

[14]. H. Sato, Y. Tsubaki, T. Hirai, and I. Komasawa, 'Mechanism of formation of metal sulfide ultrafine particles in reverse micelles using a gas injection method', Industrial and Engineering Chemistry Research, 36, 1997, pp. 92-100.

[15]. E. E. Carpenter, J. A. Sims, J. A. Wienmann, W. L. Zhou, and C. J. O'Connor, 'Magnetic properties of iron and iron platinum alloys synthesized via. microemulsion techniques', Journal of Applied Physics, 87, 9, 2000, pp. 5615-5617.

Chapter 3

Experimental section

Water-AOT-Brij 30-isoctane is used as the templating system for synthesizing gold nanoparticles. This chapter has been divided into two sections. The first part focuses on the experimental set-up used for synthesizing gold nanoparticles in this study. The second part deals with the merits and demerits of the characterization techniques used namely Dynamic Light Scattering (DLS), UV-visible spectroscopy, and Transmission Electron Microscopy (TEM). The interpretation of the average particle size (based on DLS or TEM) reported in the subsequent chapters is also discussed in this chapter.

3.1 Synthesis of gold nanoparticles

The metal precursor chloroauric acid ($HAuCl_4.3H_2O$), surfactant sodium 2-ethylhexylsulfosuccinate (AOT) and co-surfactant poly (oxyethylene)-4-laurylether (Brij 30) were obtained from Sigma Chemical Co. The reducing agent, hydrazine hydrate was obtained from S.D. Fine-chem. Ltd. The solvent (HPLC grade), isooctane was obtained from Merck Co. All the chemicals were used without further purification. De-ionized water (Millipore) was used throughout the work. All glassware were cleaned with freshly prepared aquaregia (mixture containing 1 part of HNO_3 and 3 parts of HCl, volume basis), and rinsed with tap water, de-ionized water and ethanol.

A mixed reverse micellar solution of isooctane/AOT /Brij 30 was prepared. Then, a required volume of aqueous gold chloride solution was added to the micellar solution so as to obtain the required molar ratio of water to surfactant (W_0). Similarly, mixed reverse micellar solution containing hydrazine hydrate was prepared with the same W_o ratio. The concentration followed for preliminary study was based on the values reported in the literature elsewhere [1]. The exact concentration for a particular set of experiments is mentioned in the respective sections.

Gold nanoparticles were synthesized by injecting micellar solution containing hydrazine hydrate to a micellar solution containing gold chloride using the stepper motor

device, developed by Mr. Prakash, Project Assistant in Interface Lab, Department of Chemical Engineering, Indian Institute of Science. A schematic of this set-up is shown in Figure 3.1

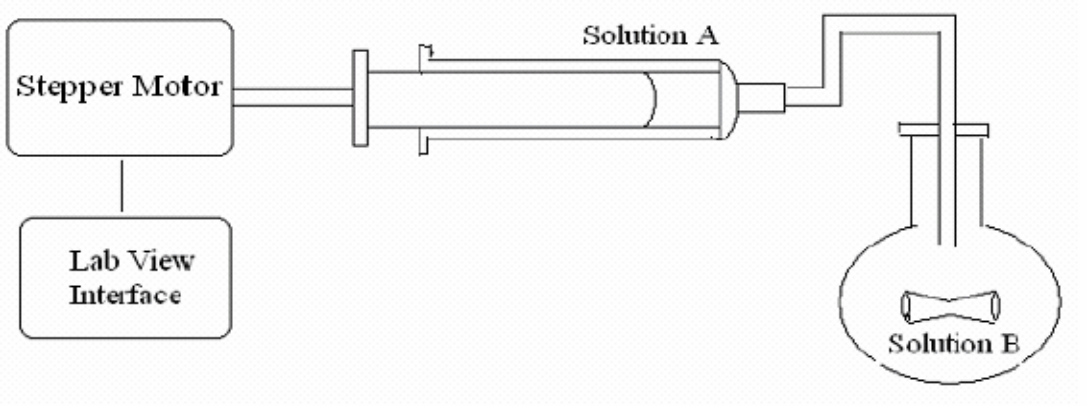

Fig. 3.1: Schematic of the experimental set-up showing the injection of hydrazine reverse micellar solution (A) to the gold chloride reverse micellar solution (B) using a stepper motor device [2].

3.2 Sample characterization

The delayed emergence of nanotechnology vis-à-vis biotechnology as a research field is due to a lag in the invention of characterization tools. For example, in the case of Atomic Force Microscopy (AFM), the force or the distance has to be measured in nN or nm. Hence, the noise level in the system has to be of the order of piconewtons or picometers. This makes the characterization of nanoparticles difficult. However, the development of newer technology like piezo-controllers has made characterization feasible now. Many characterization techniques have been developed, each having its own advantages and disadvantages. Dynamic Light Scattering (DLS), Transmission Electron Microscopy (TEM), Atomic Force Microscopy (AFM), UV-visible Spectroscopy are few of the commonly employed characterization tools for determining particle size and its distribution. TEM is an imaging technique that provides direct information while DLS is an indirect technique. In the case of TEM, only a representative sample is analyzed and this may not represent the entire sample population while in the case of DLS, performance is affected badly due to the presence of polydisperse particles. UV-visible spectroscopy is used for relatively comparing the

particle size between samples. A quantitative measurement of particle size using this technique is not feasible for all materials. Hence, an accepted method of characterization is to compare the results from different characterization techniques [3]. In this study, the characterization techniques employed are DLS, UV-visible Spectroscopy and TEM.

3.2.1 Dynamic Light Scattering (DLS)

Dynamic light scattering (DLS) is used to measure the size and distribution of particles especially in the nanometer range. DLS is also denoted as Photon Correlation Spectroscopy (PCS) and Quasi-elastic Light Scattering (QELS) [4]. DLS applies only to particles which are small enough to be suspended in a liquid and undergo Brownian motion. For example, microemulsions, liposomes, latexes, etc., are generally characterized through DLS [3].

3.2.1.1 Set-up

DLS comprises of four parts namely source, sample cell assembly, detector optics and digital correlator [5], as shown in Figure 3.2.

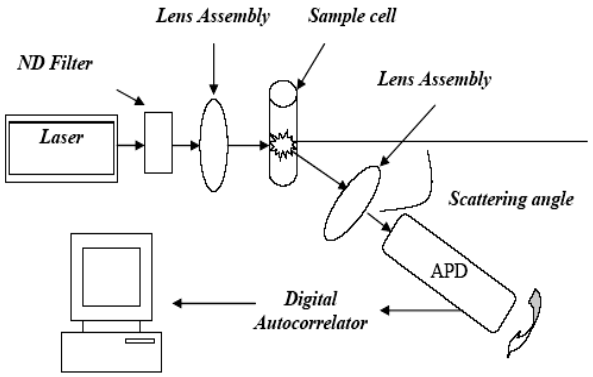

Fig. 3.2.: Schematic representation of DLS set-up

A He-Ne laser (Model: Melles Griot 75 mW; length: 1 m; operated at 632.8 nm) is used as the source. The laser passes through a neutral density (ND) filter (with an optical density of 3) for varying the power of the beam and a lens assembly which focuses the beam to the sample cell assembly. An ideal ND filter reduces light of all wavelengths equally. They are generally quantified with the help of optical density

(absorbance units/cm). In brief, higher the value of optical density, lower is the transmittance. The sample cell is surrounded by index matching liquid, decahydronaphthalene (Decalin) to reduce stray light. The index matching liquid is kept inside the vat, a cylindrical vessel. The scattered light from the sample cell assembly is detected with the help of detector optic assembly. The front portion of the detector optic assembly consists of an eyepiece which focuses the light onto an aperture. The pinhole wheel is used to change the aperture size. The filter wheel is used to allow the beam of desired wavelength. The filtered beam then passes to an avalanche photodiode (APD) which detects the temporal fluctuations of the scattered light intensity from the sample. These fluctuations are then fed to a digital auto-correlator.

In this work, Dynamic Light Scattering (DLS) instrument [Model BI-200SM] from Brookhaven Co. with BI-9000AT correlator system is used for obtaining autocorrelation function. It has an adjustable delay range, capable of producing continuous correlation function starting from 100 ns. The mean particle size and polydispersity is estimated by either the method of cumulants or packages for inverse Laplace transform like nonnegatively constrained least-squares (NNLS), CONTIN etc.

3.2.1.2 Principle of operation

Briefly, the focused beam from a laser source impinges upon particles that are undergoing random Brownian motion. As a result, the scattered light fluctuates with time at a given scattering angle which is collected by an avalanche photodiode (APD). At any given instant, the total scattered light intensity at a given scattering angle depends on the position, shape and size of the particles within the scattering volume. The total scattered intensity detected by the detector must be equal to the sum of scattered intensity by all particles (independent particles). If the concentration of the sample is too high, then the intensity detected by the detector is less than sum of the individuals, because of the interaction between particles. These temporal fluctuations of the intensity are correlated using digital auto-correlator to obtain diffusion coefficient D_t (see section 3.2.1.3).

The hydrodynamic diameter d_H is then obtained with the help of Stokes-Einstein equation,

$$D_t = \frac{K_B T}{3\pi\eta d_H} \tag{3.1}$$

where K_B is the Boltzmann's constant, η is the viscosity of sample at temperature T.

3.2.1.3 Determination of diffusion coefficient [5]

The second order auto-correlation function (ACF) is given by,

$$C(\tau) = < n(\tau)n(t-\tau) > \tag{3.2}$$

where, $n(\tau)$ is the number of photons counted over a sampling interval $\Delta\tau$ centered at time t and $n(t-\tau)$ is the number of photons counted over $\Delta\tau$ but delayed in time by τ. Then, Seigart relation is used, which is given by

$$C(\tau) = B\left(1 + f\left|g(\tau)\right|^2\right) \tag{3.3}$$

For a monodisperse sample,

$$g(\tau) = \exp(-\Gamma\tau) \tag{3.4}$$

and

$$\Gamma = D_t q^2 \tag{3.5}$$

where, Γ refers to the line width of the frequency broadened distribution of the scattered light. 'q' refers to the amplitude of the scattering wave vector, which depends on the refractive index of the liquid, wavelength of the laser and the scattering angle.

In the case of dispersions being polydisperse (particles with a distribution of sizes rather than a single size), there is a distribution of diffusion coefficients. The particles of a particular size class contribute their own exponential to the auto-correlating function (ACF). Thus, the correlation function is now a sum of exponentials.

There are many algorithms like 'method of cumulants', 'NNLS', 'CONTIN' etc., to interpret the correlation function, as a sum of exponentials. In the cumulants method, the logarithm of the ACF is expanded as a power series with time. The coefficients are the cumulants. The first cumulant is equal to the reciprocal of the average relaxation time. The second cumulant is a measure of variance. The ratio of second cumulant to the square of the first cumulant is referred to as 'poly'. If the second and higher order

cumulants are zero, the ACF is a single exponential. Alternatively, an inverse Laplace transform of the data is used to obtain the distribution function. Different software packages like NNLS, CONTIN are used to get an estimate on the particle size distribution.

3.2.1.4 Factors affecting DLS performance [5]

The fluctuations in the average count rate (ACR) must be minimized as it affects the auto-correlation function, which affects the computed particle size and distribution. An intermediate jump in the ACR represents the presence of dirt in the sample or in Decalin, the index matching liquid. The ACR should decrease with dilution of the sample with continuous phase. An increase of ACR with dilution indicates the presence of multiple scattering. In that case, the temporal fluctuations of the intensity are not random. In view of precluding multiple scattering, the sample has to be diluted until the ACR decreases with dilution. However, too much dilution can make ACR very low. The recommended value of ACR must be in between 10 kcps and 200 kcps. This can be obtained by adjusting either ND filter or pinhole wheel or filter wheel. Also, a plot of ACR with measurement time should not have any slope. Slope indicates the presence of interparticle aggregation.

In the correlator control window, baseline difference is reported. Baseline difference refers to the difference between the measured baseline and the calculated baseline. Calculated baseline is obtained from a fit of the data using Seigart relationship, and is compared with the measured baseline of long τ, delay time. Baseline difference is a measure of the quality of the sample. The baseline difference must be positive and less than 1%. A negative baseline difference can be avoided by increasing the sample measurement time. Also, high baseline difference indicates the presence of bigger size particles, probably dirt. This can be avoided only by careful sample filtration to remove dirt from the scattering volume.

Hydrodynamic diameter is based on the Stokes-Einstein equation which depends on physical properties like temperature and viscosity of the sample. Hence, these properties can also affect the noise level in the result, but their effect is not as significant as dirt.

The other parameter which can affect DLS performance is delay time. There are two delay times namely initial and final. The random motion of the particles becomes correlated when the delay time is small. As is well known, smaller particles diffuse faster when compared to bigger particles. Hence, delay time for the smaller particles must be small when compared with the big particles. The initial delay and final delay times has to be chosen in such a way that a smooth exponential decaying ACF is obtained. For sub-micron size particles, initial delay times must be in the range of 2 to 5 μs while final delay time must be of the order of few seconds.

3.2.1.5 Sampling procedure

For DLS characterization, sample cells were cleaned with 2 % Micron-90 solution (Cole-Parmer) at 60 °C, followed by de-ionized water and ethanol. The samples were used without any filtration. Multiple scattering and interparticle aggregation effects were eliminated by using appropriate concentration of the sample. Interpretation of DLS depends on Brownian motion and light scattering. Hence, to characterize the sample under true Brownian motion, concentration of the sample was decreased until the intensity detected by the detector decreases with dilution (to preclude multiple scattering). The results with baseline difference of less than 1 % were only considered for analysis. The NNLS intensity plot was used to analyze data because, when the intensity plot is converted to a number density plot, based on Rayleigh scattering, the higher modes generally vanish. Hence, to obtain results without any bias, intensity plot (actual measured value) was used and the peak height was used in selecting the dominant mode, keeping in mind the effect of size on scattered intensity. A Gaussian curve was fitted to the dominant mode using Origin software for the intensity weighted particle size distribution obtained using DLS. The software gives mean (μ) and linewidth (Γ). From linewidth, standard deviation (σ) was calculated using the relation $\sigma = 0.849\ \Gamma/2$ [6]. The percentage polydispersity is obtained as $\sigma*100/\mu$. The results reported in the preliminary study (chapter 4) are based on single DLS measurement. However, the results in the subsequent chapters have been based on six DLS measurements. A number six was chosen based on the internal standard, ISO 13321 (Particle size analysis–Photon correlation spectroscopy) [7]. The results in parametric study (chapter 6), are based on

three repetitive trials, which in turn comprises of eighteen measurements. From the eighteen DLS measurements, the results are reported with mean along with the standard error with 95 % confidence level. Further, similar procedure is employed for calculating polydispersity.

3.2.2 UV-visible Spectroscopy

Michael Faraday was the first to recognize that the red color of colloidal gold is due to metallic gold in colloidal form [8]. Nevertheless, Mie was the first to explain this phenomenon theoretically in 1908 by solving Maxwell's equation for absorption and scattering of electromagnetic radiation by spherical particles [8]. The light absorption by metallic nanoparticles can be attributed to the coherent oscillation of the conduction band electrons induced by electromagnetic field. These collective oscillations are known as surface plasmons. This effect is treated as small particle effect, as this cannot be seen either in atoms or bulk. This occurs due to confinement of electrons in the nanoparticle. In recent years, probing of particle shape, size and its distribution using Surface Plasmon Resonance (SPR) has gained a lot of momentum. In literature, the variation of peak position with particle size has been documented [8]. The wavelength at which SPR occurs can be used for characterization of nanoparticles. In the case of gold, the SPR occurs in the visible regime, which can be detected by UV-visible spectroscopy. In this study, UV-visible spectrometer from Shimadzu was employed for sample characterization. A known sample dilution (1 ml of sample to 2 ml of isooctane) was used and scanned over a wavelength ranging from 200 nm to 900 nm with a resolution of 0.5 nm. For gold nanoparticles, the solvent, isooctane was used for background subtraction.

The raw data is then processed using origin software to obtain absorbance peak, λ_{max}. Further, the area under the SPR between 400 to 650 nm is obtained after excluding Mie background. The significance of area under the SPR peak in the UV-visible spectra is discussed in the next chapter.

3.2.3 Transmission Electron Microscopy

Transmission Electron Microscopy (TEM) operates on the same principle as the light microscope. In light microscope, light is used to image particles while in TEM,

electrons are used. In the case of optical microscope, the resolution is limited by the wavelength of the light. However, the use of electrons in TEM has made possible image resolution of the order of Angstroms. In TEM, electrons are directed towards sample, which travel through vacuum from the top of microscope. Electromagnetic lenses are used to focus the electrons into a collimated beam. Some electrons are transmitted through sample depending on the specimen under analysis. The transmitted electrons fall on the fluorescent screen located at the bottom of the microscope and form the image.

TEM analysis (using Tecnai F30, Nanoscience initiative center, Indian Institute of Science) was performed on a few randomly chosen samples and the results are presented in Appendix 3. Samples for TEM were prepared by placing 12 drops of the sample on a carbon grid placed on tissue paper and then washing with acetone (HPLC grade). This procedure was repeated again to attain a reasonable density of particles on the carbon film, and then the sample was used for analysis. For obtaining particle size and distribution from TEM, Clemex software (Clemex Vision PE) was used. After setting the scale bar, the image was converted to binary format using grey threshold. This process was done manually. After binary operation, 'separate' command is used to isolate particles. It is a morphological filter that separates features by distance analysis. An example of an image before and after separate operation is shown in Figure 3.3.

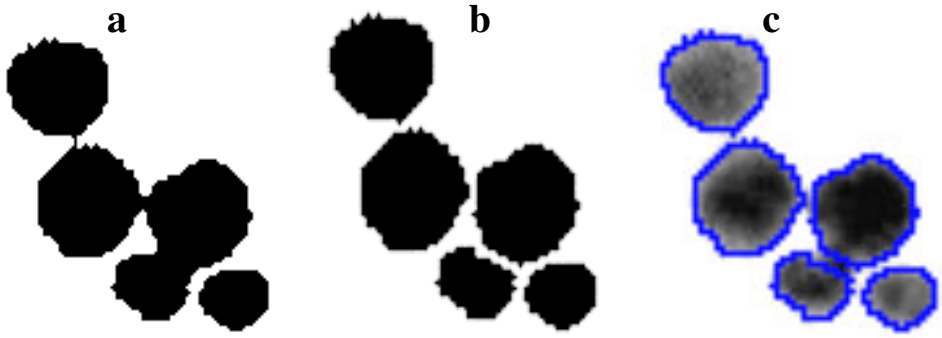

Fig. 3.3: Example of image processing induced artifacts. a) Binary image before separation, b) after separation, c) the thresholded image along with an outline of the threshold.

For particle size and distribution, the circular diameter is used. The circular diameter is calculated from the particle area (using pixels). For particular sample, different images were obtained at different locations on the TEM grid along with

different magnifications. These images were then analyzed using Clemex software. The particle size and distribution of all images from a particular sample is averaged. The standard deviation reported in this study is 'pooled standard deviation'.

3.3 Conclusions

The main aim of this chapter is to recognize the merits and demerits of characterization techniques employed for determining particle size and distribution. A brief overview on various characterization techniques employed in this study was discussed. Even though, TEM is a direct imaging technique, the sample analyzed does not represent the entire population On the other hand, DLS along with UV-visible spectroscopy gives information about the entire sample. Hence, in this study, TEM is used to support DLS results. Also, in this chapter, nuances associated with DLS measurements were presented and discussed.

3.4 References

[1]. C. L. Chiang, 'Controlled growth of gold nanoparticles in AOT/$C_{12}E_4$/Isooctane mixed reverse micelles', Journal of Colloid and Interface Science, 239, 2001, pp. 334–341.

[2]. D. Surya, 'Synthesis and characterization of gold nanoparticles', Master of Engineering report, Indian Institute of Science, 2006**.**

[3]. M. A. Michaels, 'Quantitative model for the prediction of hydrodynamic size of nonionic reverse micelles', Master of Science report, Virginia Commonwealth University, 2006.

[4]. B. B. Weiner, 'Particle sizing using ensemble averaging techniques', Brookhaven Instruments Corporation (BIC), pp. 155-171.

[5]. Instruction manual for BI-200SM Goniometer Version 2.0, Third print, Brookhaven Instruments Corporation (BIC), 1993.

[6]. http://hyperphysics.phy-astr.gsu.edu/hbase/math/gaufcn2.html#c1 accessed on 9/1/2007.

[7]. International standard, 'ISO 13321: Particle size analysis-Photon correlation spectroscopy', First edition, 1996-07-01.

[8]. S. Link and M. A. El-sayed, ‘Spectral properties and relaxation dynamics of surface plasmon electronic oscillations in gold and silver nanodots and nanorods’, Journal of Physical Chemistry B, 103, 1999, pp. 8410-8426.

Chapter 4

Exploratory study

There were issues related with reproducibility, the role of co-surfactant and stability of nanoparticles synthesized in on earlier work [1]. Hence, exploratory experiments were carried at concentration of the reactants and surfactants as reported in the literature [2]. These experiments were carried in a 50 ml round bottom flask with the help of magnetic stirrer. AOT and Brij 30 concentration was 0.1 M and 0.2 M respectively. Typically, 10 ml of reverse micellar solution of reducing agent was added at different rates to a 10 ml reverse micellar solution of gold salt. A preliminary experiment was performed to determine the time needed for completion of the reaction. DLS measurement was carried out on an aliquot of the solution after every five minutes. The effective diameter of the nanoparticles was obtained as 52, 55, 55 nm at the end of 5, 10 and 15 minutes respectively. Also, visual observation (based on color change) indicated that the reaction was complete after ten minutes. Hence, a mixing time of twelve minutes was chosen for all further experiments in order to allow for complete reaction. Various parameters like concentration of gold chloride salt, ratio of reducing agent to precursor concentration, addition rate of reducing agent were varied to study their effect on particle size.

4.1 Effect of addition rate

In order to study the effect of addition rate of reducing agent on particle size independently, experiments were carried at room temperature (26 ± 1 °C). The results are tabulated in Table 4.1. From the results, it can be inferred that the effect of addition rate of reducing agent is not that significant on particle size for reactant concentrations similar to that of previous study [1]. The samples were not stable and became clear within a day. The experiments were reproducible within experimental errors based on DLS characterization.

Hydrazine addition rate (ml/s)	Average particle size (nm), [% PD]; Trial 1	Average particle size (nm), [%PD]; Trial 2
0.50	9, [25]	10, [25]
0.33	5, [16]	8, [31]
0.25	7, [20]	-
0.17	9, [28]	-

Table 4.1: DLS measurements of the effect of hydrazine addition rate on particle size. Synthesis conditions: [$HAuCl_4$]: 0.05 M; [N_2H_5OH]: 0.125 M; [AOT]: 0.1 M; [$C_{12}E_4$]: 0.2 M; W_o: 8 including co-surfactant; % PD (polydispersity) refers to the percentage variation of standard deviation with respect to the mean size.

4.2 Effect of mixing volume

Mixing patterns are also expected to play a significant role in nanoparticle synthesis using microemulsions [3]. In view of verifying this, an experiment was carried with half of the total reagent volume (5 ml of gold chloride reverse micellar solution and 5 ml of hydrazine reverse micellar solution) with all other conditions remaining the same as reported in section 4.1. The results (in Table 4.2) indicate that particle size is drastically affected by mixing patterns. Subsequently, the experiments carried during preliminary studies were conducted with a final reaction volume of 20 ml.

Hydrazine addition rate (ml/s)	Total volume of reactants (ml)	Size (nm), [%PD]
0.17	20	9, [28]
0.17	10	16, [14]

Table 4.2: DLS measurements of the effect of total volume of reactants on particle size. Conditions: [$HAuCl_4$]: 0.05 M; [N_2H_5OH]: 0.125 M; [AOT]: 0.1 M; [$C_{12}E_4$]: 0.2 M; W_o: 8 including co-surfactant. % PD (polydispersity) refers to the percentage variation of standard deviation with respect to the mean size.

4.3 Stability of nanoparticle solution

Another aspect of all these samples was that their stability was poor. Within a few days, nanoparticle agglomerates were seen to be deposited as a black powder at the bottom, while the solution became clear. These could be re-dispersed to form a pink solution after shaking. However, the ability to re-disperse also reduced with time. This

indicated that there were some issues regarding the stabilization of the nanoparticles. A UV-visible spectrum was performed over the complete spectral range and to our surprise we observed a peak around 280 nm as shown in Figure 4.1. This corresponds to the presence of gold chloride ions in the solution. This was unexpected as there was three times excess of reducing agent compared to stochiometric requirements (Equation 1.1). From this it can be inferred that some side reactions were taking place. Clint et al. have reported the formation of an imine due to the reaction of AOT with hydrazine as shown in Figure 4.2 [4].

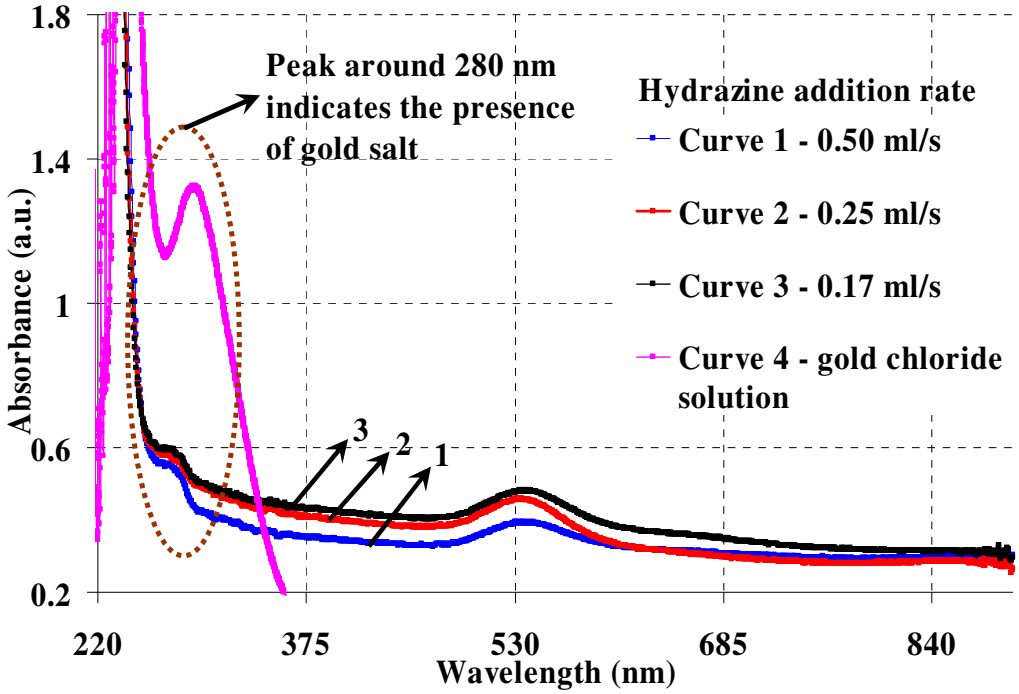

Fig. 4.1: UV-visible spectra of gold nanoparticle solutions synthesized at various hydrazine addition rates. Conditions: [$HAuCl_4$]: 0.05 M; [N_2H_5OH]: 0.125 M; [AOT]: 0.1 M; [$C_{12}E_4$]: 0.2 M; W_o: 8 including co-surfactant. The outlined region (oval shaped) is used to highlight the presence of a peak around 280 nm (gold chloride ions).

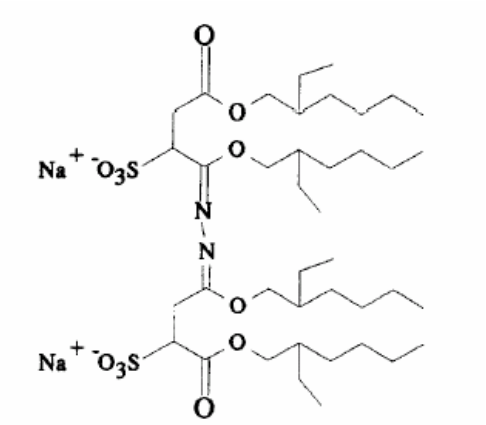

Fig. 4.2: Chemical structure of AOT dimer formed due to the reaction of AOT with hydrazine [4]

4.4 Effect of reactant concentrations

In view of verifying the hypothesis of side reaction, reducing agent concentration was increased from 0.125 M to 0.5 M (12 times more than the stochiometric requirements). Now, there was no peak around 280 nm in the UV-visible spectra indicating the complete reduction of gold ions in solution. The results were found to be reasonably reproducible within experimental errors. The Surface Plasmon Resonance peak in the UV-visible spectra also shifted in accordance with the DLS results, thereby indicating that measurements made using DLS were reliable. Also, the results indicated no drastic effect of addition rate of hydrazine on particle size. The absorbance peak position in the UV-visible spectra is in the range of 522 to 530 nm for all the samples. A sample UV-visible spectrum is shown in Figure 4.3. The spectra for the remaining samples are presented in Appendix 2. The effect of gold chloride concentration on particle size and its distribution at a fixed reagent ratio of 10 (hydrazine to gold chloride, molar basis) is presented in Table 4.3.

In order to study the effect of decreasing gold concentration, maintaining a constant ratio of reducing agent to precursor concentration, the gold chloride concentration was decreased by a factor of four from 0.05 M to 0.0125 M. The results were seen to be reasonably reproducible within experimental errors. Again, there wasn't any drastic change in the variation of particle size with reagent addition rate. The UV-visible peak for all the samples is in the range of 529 to 540 nm. The absence of peak at 280 nm indicated the complete reduction of Au^{3+} ions

Gold chloride concentration (M)	Hydrazine addition rate (ml/s)	Average particle size (nm), [% PD], Trial 1	Average particle size (nm), [% PD], Trial 2
0.05	0.50	6, [16]	11, [18]
0.05	0.33	15, [10]	11, [13]
0.05	0.25	10, [10]	15, [29]
0.05	0.17	18, [26]	12, [08]
0.05	0.11	12, [05]	18, [12]
0.05	0.07	18, [12]	17, [13]
0.05	0.04	19, [12]	18, [13]
0.05	0.03	18, [13]	18, [17]
0.0125	0.50	14, [19]	8, [12]
0.0125	0.33	11, [12]	11, [09]
0.0125	0.25	15, [12]	12, [09]
0.0125	0.20	-	17, [22]
0.0125	0.17	16, [19]	16, [14]
0.0125	0.13	-	8, [19]
0.00625	0.50	9, [17]	-
0.00625	0.33	10, [19]	-
0.00625	0.25	10, [14]	-
0.00625	0.20	7, [13]	-
0.00625	0.17	9, [17]	-
0.00625	0.13	11, [16]	
0.00625	0.11	9, [13]	

Table 4.3: Effect of gold chloride concentration and hydrazine addition rate on particle size and distribution. Conditions: Molar ratio of hydrazine to gold chloride concentration was 10 (12 times excess than the stochiometric requirements), [AOT]: 0.1 M, [Brij 30]: 0.2 M, W_o = 8, including co-surfactant. "% PD" (Polydispersity) refers to the percentage variation of standard deviation from mean. "-" indicates that the sample at the respective conditions was not prepared.

The samples were less stable as compared with the samples prepared using higher gold concentration (0.05 M). In this case, the amount of dark precipitate formed was more as observed visually, than the amount that had settled in the experiments carried out at the higher gold chloride concentration (0.05 M). In view of analyzing the effect of gold chloride concentration on the stability of nanoparticles, the concentration was reduced further from 0.0125 M to 0.00625 M, while maintaining a constant molar ratio of reducing agent to precursor salt. In this case, the effect of addition rate of reducing agent on particle size was found to be independent of addition rate within measurement errors. The particle size was found to be around 9 nm.

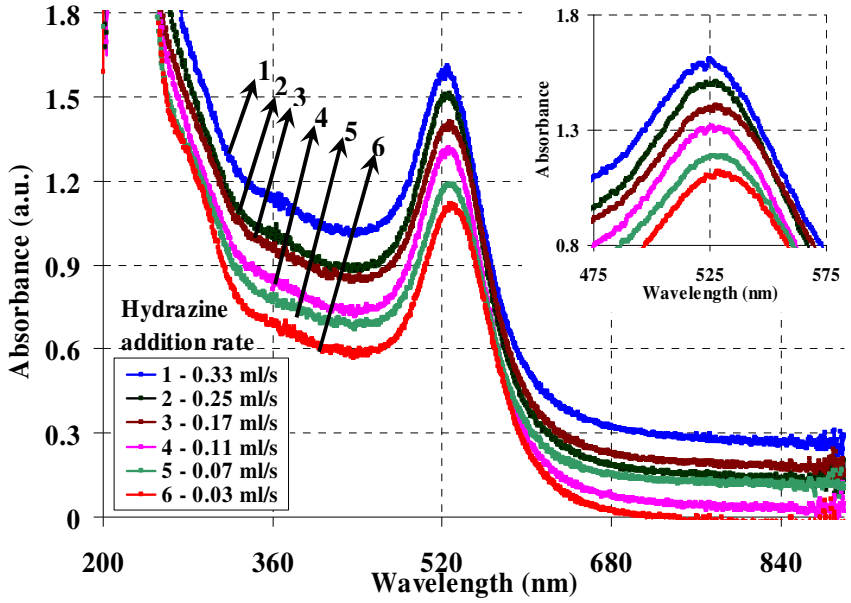

Fig 4.3: UV-visible spectra of gold nanoparticles synthesized by mixing two microemulsion solutions containing gold salt and reducing agent. Process conditions: [$HAuCl_4$]: 0.05 M; [N_2H_5OH]: 0.5 M; [AOT]: 0.1 M; [$C_{12}E_4$]: 0.2 M; W_o: 24. The inset shows a magnified view of the peak position indicating a shift from 523 to 530 nm as the hydrazine addition rate is varied from 0.33 ml/s to 0.03 ml/s.

The UV-visible spectrum shows a broad peak around 530 nm for all the samples. Again, visual inspection indicated that the amount of dark precipitate settled was more than the previous samples. Hence, this indicates that concentration of gold chloride indeed plays a role in stability of particles in solution. This may be attributed to the role of chloride ions in stabilizing the nanoparticles within the water pools during the growth.

4.5 Quantification of yield and stability of nanoparticles in solution

The area under the Surface Plasmon Resonance (SPR) in the UV-visible spectra was obtained for all the samples. Based on trial and error, it was found that the region between 400 and 650 nm matches well with the background when compared with other regions. A sample curve is shown in Figure 4.4. Thus, for all the samples the area was calculated between 400 and 650 nm. For a particular gold chloride concentration, the area was calculated by averaging all the data points at different addition rates, since the size variation was less than 20 nm and the UV-visible peak position were relatively constant. This plot is shown in the Figure 4.5. The area under the SPR peak gives an estimate of the amount of gold nanoparticles present in the solution and so can be used as an indicator for assessing the relative yield of nanoparticles. As the gold chloride has been completely reduced in these experiments, the trend line matches well with the data points.

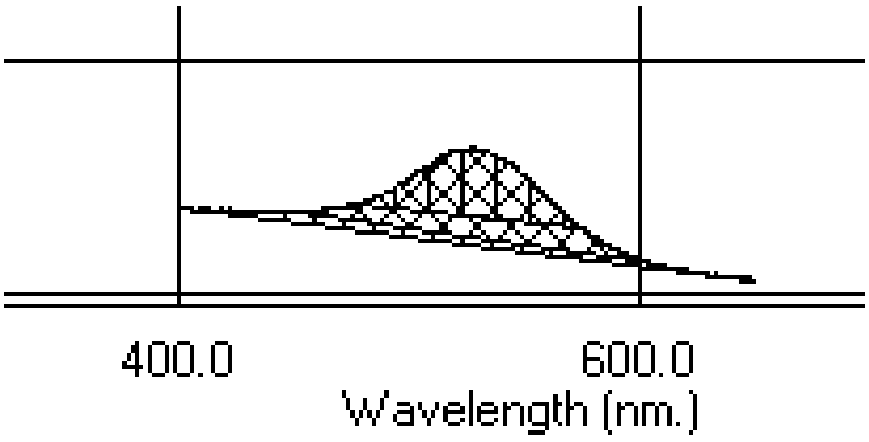

Fig. 4.4: Plot showing area under the SPR peak in the UV- visible spectra for sample for different wavelength regions.

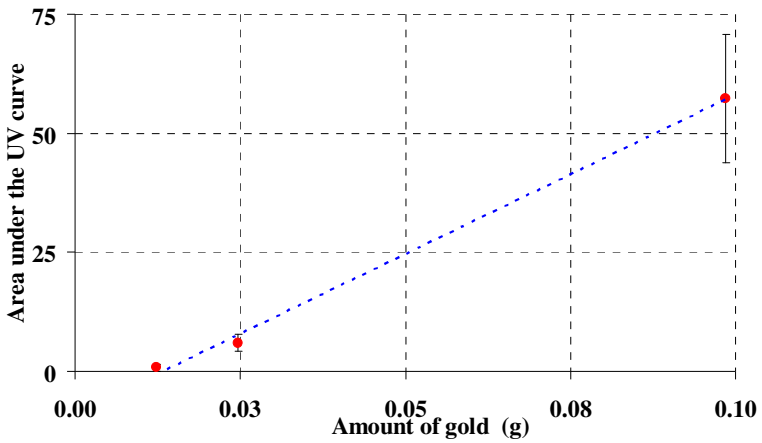

Fig. 4.5: Plot showing the effect of gold concentration on the area in the UV-visible spectra under the SPR peak between 400 and 650 nm. The error bars indicate standard deviation.

The UV- visible analysis was repeated for few randomly chosen samples after one month and the area under the SPR between 400 to 650 nm was compared with the original sample. The results are tabulated in Table 4.4. From the results, it can be inferred that gold concentration plays a vital role for the stability of the sample. The peak also became broader for samples synthesized at reduced gold chloride concentrations, indicating higher polydispersity.

Gold chloride concentration (M) [Sample ID]	**Initial area (arbitrary units)**	**Final area (arbitrary units)**	**% area decrease** $\left(\frac{\text{Initial}-\text{Final}}{\text{Initial}}\right)*100$
0.05 [MG 39]	64.00	58.96	7.8
0.05 [MG 52]	60.19	58.28	3.2
0.05 [MG 53]	64.79	57.00	12.0
0.0125 [MG 46]	6.24	4.51	27.8
0.0125 [MG 61]	5.81	4.89	15.9
0.0125 [MG 67]	7.57	5.53	27.0
0.00625 [MG 78]	0.48	0.24	49.7

Table 4.4: Effect of gold chloride concentration on decrease in area under the SPR peak in the UV- visible spectra of nanoparticle solutions after one month.

4.6 Conclusions

The main aim of synthesizing stable gold nanoparticles using microemulsions was achieved. The reasons for attaining stable nanoparticles are attributed to a better synthesis protocol (cleaning glasswares with aquaregia) resulting in minimizing heterogeneous nucleation and to an increase in the amount of excess reducing agent by a factor of twelve as compared to three. Based on this exploratory study, it was also found that aging is not a necessary condition for synthesizing gold nanoparticles using microemulsions as reported [1]. The variability in pervious study can be attributed to the side reaction between surfactant (AOT) and reducing agent (Hydrazine) resulting in varying amounts of reducing agent available for reaction. Several parameters were varied to study their effect on particle size and distribution. An increase in total reagent volume decreases the particle size, but increases polydispersity at constant hydrazine addition rate, reactant concentrations and temperature. At higher gold chloride concentrations (0.05 and 0.0125 M), a decrease in hydrazine addition rate results in an increase of the particles size, while at low concentration (0.00625 M), the particle size remains constant around 9 nm. However, the effect of addition rate on polydispersity is uncorrelated, irrespective of gold chloride concentrations. The area under the SPR peak in the UV-visible spectra between 400 to 650 nm can be used as an indicator for assessing the relative yield of nanoparticles in solution. Further, the same parameter can be used to quantify stability of the colloidal solution (by analyzing after few weeks). It was found that an increase in gold chloride concentration increases the stability of nanoparticles in solution.

Nevertheless, there is a discrepancy between the initial micelle size and final particle size. Also, the role of co-surfactant is not well understood. Thus, a careful study on reverse micelle size is warranted, the results of which are discussed in the following chapter.

4.7 References

[1]. D. Surya, 'Synthesis and characterization of gold nanoparticles', Master of Engineering report, Indian Institute of Science, 2006.

[2]. C. L. Chiang, 'Controlled growth of gold nanoparticles in AOT/$C_{12}E_4$/Isooctane

mixed reverse micelles', Journal of Colloid and Interface Science, 239, 2001, pp. 334–341.

[3]. R. Singh, S. Kumar, 'Effect of mixing on nanoparticle formation in micellar route', Chemical Engineering Science, 61, 2006, pp. 192-204.

[4]. J. H. Clint, I. R. Collins, J. A. Williams, B. H. Robinson, T. F. Towey, P. Cajean and A. K. Lodhi, 'Synthesis and characterisation of colloidal metal and semiconductor particles prepared in microemulsions', Faraday Discussions, 95, 1993, pp.219-233.

Chapter 5

Reverse micelle study

In all the experiments carried out as part of the exploratory study (chapter 4), the minimum particle size formed was 8 nm, and the size of the reverse micelle corresponding to a W_o of 8 (based on total moles of surfactant and co-surfactant) is expected to be 6 nm [1, 2]. In view of investigating the above discrepancy and the effect of co-surfactant, a systematic study using DLS characterization of the size of mixed reverse micelle as a function of preparatory conditions was carried out. In literature, DLS characterization has been based on two methods [3]. The first method involves the characterization of the original sample without dilution and the resulting diameter is treated as apparent hydrodynamic diameter [3]. Then to get an estimate of the real hydrodynamic diameter, correlations are used that account for dispersed phase volume fraction and interactions between the micelles. The other technique involves the determination of micelle size at various dilutions, and then extrapolating the diameter to infinite dilution [3]. The problem with the former technique involves the use of theoretical correlations, which do not apply at higher water to surfactant molar ratios, while the latter technique may result in a change of phase.

Initially, the reverse micelles were prepared with gold chloride ions as required for the reaction. However, the average scattered intensity detected continued to increase with time upon dilution of the original micellar solution. The reasons for this increase are not clear at the moment. However, this was not observed without the ions in the solution. So, DLS characterization of swollen reverse micelles was carried out using de-ionized water only. In following sections, the effect on reverse micelle size of various parameters like sonication, surfactant concentration will be discussed along with the role of co-surfactant in nanoparticle synthesis. Finally, issues related with scaling up of the system are discussed.

5.1 Effect of sonication on micelle size

The minimum number of components required to form a microemulsion is three. In this study, water-AOT-isooctane was used. The size of the reverse micelles was characterized using DLS. In literature, it has been reported that sonication during microemulsion formation helps in reducing the polydispersity of reverse micelles [4]. The process of solubilization of surfactant in organic phase can be carried in two different ways, either by manual methods (micelles without sonication) or aided with sonication (micelles with sonication). The surfactant (AOT) solubilizes in isooctane within two minutes resulting in transparent solution. Hence, sonication time was chosen as three minutes. The study was carried out at two molar ratios of water to AOT, namely 8 and 24. The original micellar solutions were characterized first to get an estimate on apparent hydrodynamic diameter. Then, assuming that the phase diagram would not get affected with little dilution, the sample was diluted approximately 20 % (based on volume), in view of determining the presence of multiple scattering. The same level of dilution was used until the average intensity of scattered light decreased with dilution. The diameter obtained from the most dilute sample is treated as the real diameter. Hence, there would not be much difference between the size obtained here and by extrapolating to infinite dilution. The results are tabulated in Table 5.1. Results show a clear difference in the reverse micelle size between unsonicated and sonicated reverse micellar solutions. The real diameter obtained after avoiding multiple scattering effects in the case of unsonicated sample correlates well the correlation reported in the literature [1],

$$\text{Hydrodynamic diameter} = 0.35 * W_o + 3 \quad (\text{at } 25\ ^\circ\text{C})$$

However, the difference in the diameter between the sonicated and unsonicated sample is more than 30 %. Moreover, in the case of higher molar ratio of water to AOT (24), the polydispersity has increased significantly upon sonication, contrary to expectations. A careful literature survey revealed that sonication time is a crucial parameter for reducing polydispersity. Landfester et al. have reported that a minimum sonication time of 15 minutes is required for attaining steady state in the case of sodium dodecyl sulfate (SDS) miniemulsion [4]. This result is based on the time required for percenatge turbidity and surface tension to stabilize as depicted in Figure 5.1.

	Micelles with sonication	
	W_o = 8	**W_o = 24**
$D_{H,\ apparent}$ (nm); [% PD]	7.9 ± 1.3; [09]	-
$D_{H,\ real}$ (nm); [% PD]	7.6 ± 0.8; [08]	13.6 ± 1.8; [16]
	Micelles without sonication	
	W_o = 8	**W_o = 24**
$D_{H,\ apparent}$ (nm); [% PD]	5.6 ± 0.9; [07]	-
$D_{H,\ real}$ (nm); [% PD]	6.1 ± 0.3; [08]	9.4 ± 1.1; [10]

Table 5.1: Results of DLS characterization of reverse micelles formed by water-AOT-isooctane system showing the effect of multiple scattering and sonication on micelle size and distribution. The concentration of AOT is 0.1 M; "$D_{H,\ apparent}$" refers to the hydrodynamic diameter obtained from original micellar solution, while "$D_{H,\ real}$" refers to the diameter obtained after dilution to avoid multiple scattering. % PD refers to the percentage variation of standard deviation with respect to mean size. "W_o" refers to the molar ratio of water to AOT.

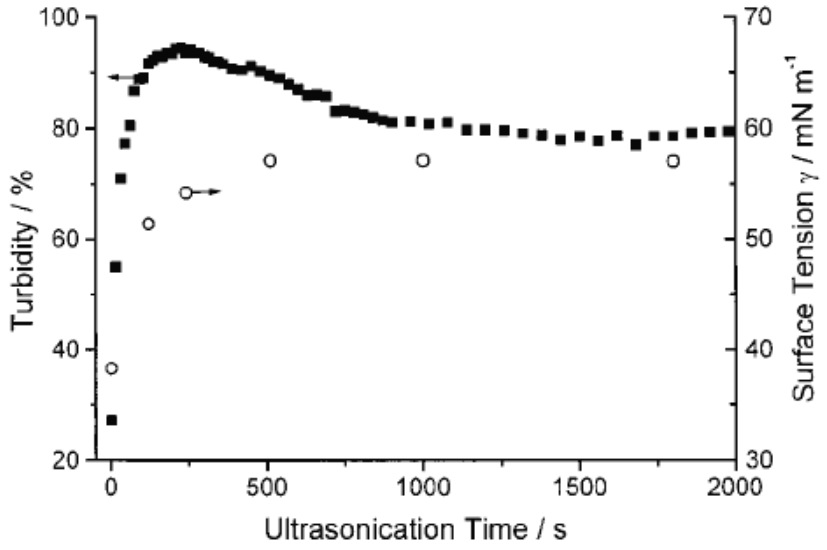

Fig. 5.1: Effect of sonication time on percentage turbidity and surface tension [4]

Hence, further experiments were carried out with a minimum sonication time of 15 minutes. The number of components was increased to four with the addition of co-surfactant, Brij 30 to emulate the desired system.

	Micelles with sonication	
	W_o = 8	**W_o = 24**
$D_{H, apparent}$ (nm), [%PD]	5.4 ± 1.6; [09]	7.3 ± 1.2; [11]
$D_{H, real}$ (nm), [%PD]	5.1 ± 1.8; [10]	16.7 ± 1.5; [09]
After 1 day		
$D_{H, apparent}$ (nm), [%PD]	6.4 ± 1.3; [08]	5.8 ± 0.6; [07]
$D_{H, real}$ (nm), [%PD]	5.9 ± 1.6; [10]	15.6 ± 0.7; [13]
After 2 days		
$D_{H, apparent}$ (nm), [%PD]	3.9 ± 0.7; [08]	5.6 ± 0.2; [07]
	Micelles without sonication	
	W_o = 8	**W_o = 24**
$D_{H, apparent}$ (nm), [%PD]	5.5 ± 1.1; [09]	6.4 ± 0.4; [08]
$D_{H, real}$ (nm), [%PD]	6.4 ± 0.4; [11]	10.3 ± 1.9; [11]
After 1 day		
$D_{H, apparent}$ (nm), [%PD]	3.0 ± 0.7; [07]	5.9 ± 1.2; [15]
$D_{H, real}$ (nm), [%PD]	3.4 ± 0.1; [06]	10.9 ± 0.5; [10]
After 2 days		
$D_{H, apparent}$ (nm), [%PD]	3.8 ± 1.2; [05]	5.0 ± 0.4; [04]

Table 5.2: Results of DLS characterization of reverse micelles formed by Water-AOT-Brij 30-Isooctane system showing the effect of sonication and molar ratio of water to AOT on reverse micelle size and its distribution along with its stability. Conditions: [AOT]: 0.1 M, [Brij 30]: 0.2 M. "$D_{H, apparent}$" refers to the hydrodynamic diameter obtained from original micellar solution while "$D_{H, real}$" refers to the diameter obtained after dilution to avoid multiple scattering. % PD refers to the percentage variation of standard deviation with respect to the mean size. "W_o" refers to the molar ratio of water to AOT.

Two sets of samples were prepared, one with molar ratio of water to AOT of 8 (water to total surfactant: 2) and the other 24 (water to total surfactant: 8), in order to test whether the molar ratios reported in literature the amount of co-surfactant. Also, to study the stability of the micelles, their size was measured after one day, over a total period of two days. The results are tabulated in Table 5.2. In the case of lower water to AOT molar

ratio (~8), the sonicated sample is more stable than the unsonicated sample, over a period of one day based on the micellar size. Also, the apparent and real hydrodynamic diameters are similar. However, the diluted samples are not stable for even a day, as seen by the measured change in the micellar size. In the case of high water to AOT (~24), the apparent hydrodynamic diameter obtained from the sonicated and the unsonicated sample are similar. However, after avoiding multiple scattering effects by dilution, the size difference is more than 100%. Again, the diluted samples are not stable for even one day. From these experiments, it can be inferred that sonication is required for low molar ratio of water to AOT (~8). Moreover, it is clear from these studies that molar ratio of water to surfactant, as reported in the literature does not include the amount of co-surfactant.

5.2 Effect of co-surfactant

Different co-surfactants have been employed in the literature [5]. Most co-surfactants fall under the category of either alcohols or poly (oxyethyl) alkyl ethers. Poly (oxyethyl) alkyl ethers (or Brij series) help in micellar clustering, thereby increasing the percolation (fusion of droplets); this is critical for nanoparticle synthesis. The effect of these two types of co-surfactants is shown schematically in Figure 5.2.

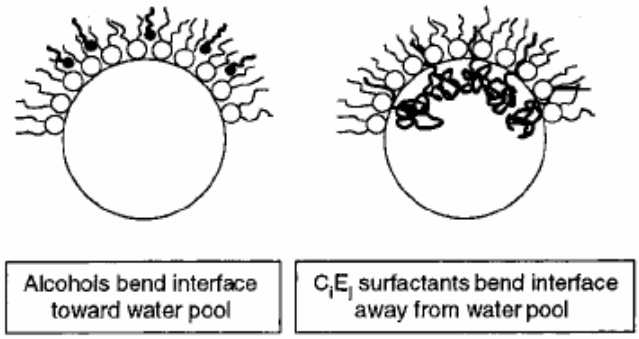

Fig. 5.2: Schematic representation of the effect of alcohol and Brij compounds on AOT reverse micelles as co-surfactants [5]

Commercially, a wide range of Brij compounds are available. The difference between the compounds is either in the size of hydrophobic tail or hydrophilic head. Based on the studies carried out by Nazario et al. three parameters affect the behavior of the micellar system namely the effect of head group size (C_i portion), tail length of co-

surfactant (E_j portion) and the molar ratio of co-surfactant and surfactant [3]. It has been reported that if the head group size is large, then the variation of size with respect to molar ratio of water to surfactant is more. Co-surfactants with smaller head group size (2 to 4) are desirable from a scaling-up point of view, as they endow AOT reverse micelles to be less sensitive to small fluctuations in process conditions and thereby improve the reproducibility of the process. It is also reported that the effect of tail length on micelle size is negligible as compared to the effects of other parameters. Based on these two parameters, the co-surfactant choice was narrowed down to either Brij 30 or Brij 52.

The molar ratio of co-surfactant to surfactant is another crucial parameter that affects synthesis of nanoparticles in reverse micelles. If the concentration of the co-surfactant is much higher than the surfactant, it results in phase separation while if the concentration of the surfactant is much higher, then it results in a liquid crystalline phase (different association structure) [6]. Hence, an optimum ratio of 0.5 was chosen as recommended by Nazario and his co-workers [5].

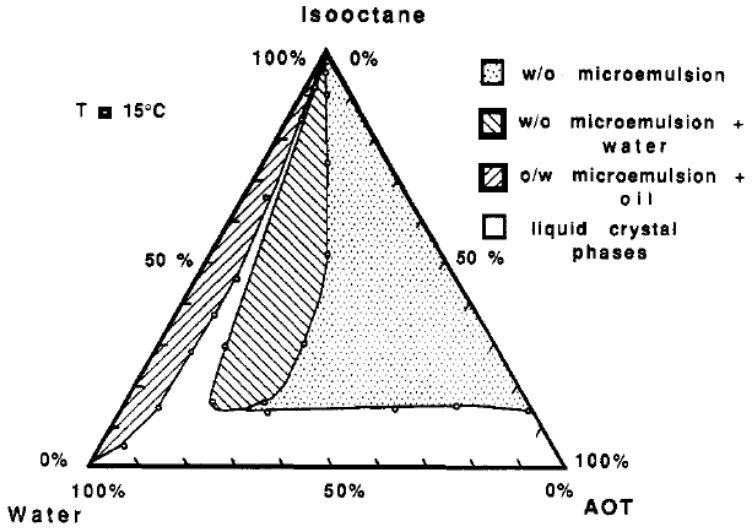

Fig. 5.3: Phase diagram of water/AOT/isooctane system at 15 °C [7]

The phase diagram of water-AOT-isooctane at 15 °C is shown in Figure 5.3 [7]. The amount of the surfactant used in the preliminary work was only 6 % (AOT). This indicates that so far the study has been carried at the boundary of microemulsion region based on the composition of reverse micellar solution. During DLS characterization, the samples need to be diluted to preclude the effects of multiple scattering. Hence, there is a

possibility of working outside the microemulsion regime. Hence, it was decided to increase the concentration of AOT, so that even with dilution, the study will be carried inside the microemulsion regime. The AOT concentration was increased to 0.2 M (such that amount of AOT is more than 10 %) and subsequently, the concentration of the co-surfactant was taken to be 0.1 M in order to maintain the ratio of co-surfactant to surfactant ratio of 0.5.

In view of choosing the right combination of surfactant and co-surfactant, the following experiments were performed. Three different sets of microemulsions namely water-AOT-isooctane, water-AOT-Brij 30-isooctane and water-AOT-Brij 52-isooctane were prepared with the water to AOT molar ratio maintained at a value of 8 in all cases. For solubilizing AOT in isooctane, making mixed microemulsion (addition of co-surfactant), and solubilizing water in mixed microemulsion, sonication times of 15, 5 and 15 minutes respectively were chosen. After forming the respective microemulsions, the samples were kept at a constant temperature of 25 ± 1 °C for ~ 60 minutes, so as to allow them to equilibrate with the room temperature. This is necessary as sonication may increase the solution temperature. The results are presented in Table 5.3.

	System I	**System II**	**System III**
$D_{H,\ apparent}$ (nm), [%PD]	6.9 ± 0.9; [09]	5.7 ± 1.4; [09]	6.4 ± 3.1; [09]
$D_{H,\ real}$ (nm), [%PD]	6.2 ± 1.1; [10]	4.9 ± 1.6; [08]	6.0 ± 0.3; [08]
After 1 day			
$D_{H,\ apparent}$ (nm), [%PD]	6.5 ± 1.3; [08]	4.1 ± 0.9; [05]	4.1 ± 0.8; [07]
$D_{H,\ real}$ (nm), [%PD]	5.4 ± 1.1; [07]	5.2 ± 0.8; [08]	4.0 ± 1.5; [08]
After 2 days			
$D_{H,\ apparent}$ (nm), [%PD]	6.2 ± 1.4; [08]	3.7 ± 0.6; [05]	9.1 ± 3.4; [10]

Table 5.3: DLS measurements of the effect of co-surfactants like Brij 30 and Brij 52 on reverse micelle size and its distribution along with its stability on water-AOT-isooctane system. System I refer to water-AOT-isooctane while system II and system III refer to water-AOT-Brij 30-isooctane and water-AOT-Brij 52-isooctane respectively. Conditions: [AOT]: 0.2 M, [Brij 30] or [Brij 52]: 0.1 M; For all systems, molar ratio of water to AOT is 8. "$D_{H,\ apparent}$" refers to the hydrodynamic diameter obtained from original micellar solution while "$D_{H,\ real}$" refers to the diameter obtained after dilution to avoid multiple scattering. % PD refers to the percentage variation of standard deviation with respect to mean size.

Based on the apparent hydrodynamic diameter, the water-AOT-isooctane system is stable for more than two days while the quaternary systems (co-surfactant) are stable for only one day. Also, the difference between the apparent and real hydrodynamic diameter is less than 10%. Within the quaternary systems, the one incorporating Brij 30 seems to be more stable than Brij 52 based on real hydrodynamic diameter. Further, aging of diluted micellar solution results in degradation of the sample within a day (based on reverse micelle size). Based on this study, it was concluded that Brij 30 is the right choice as co-surfactant for synthesizing nanoparticles.

5.3 Gold nanoparticle synthesis in ternary system

In this study, water-AOT-isooctane was used as the templating system for synthesizing gold nanoparticles. The main objective of this study was to compare this system with the quaternary system reported in literature [8]. At first, 0.1 M aqueous gold chloride solution, 1 M hydrazine solution and 0.1 M AOT in isooctane were prepared. Then, a required volume of aqueous gold was added to the AOT/isooctane reverse micellar solution to obtain water to AOT molar ratio of 8. Similarly, hydrazine reverse micellar solution was prepared with the same water to surfactant ratio. Nanoparticles were synthesized by injecting 10 ml of hydrazine reverse micellar solution to 10 ml of micellar gold chloride solution at different rates. The results of DLS characterization are presented in Table 5.4. The UV-visible spectra of the samples are presented in Figure 5.4.

Hydrazine addition rate (ml/s)	**Size (nm)**	**λ_{max} (nm)**
0.50	4, [30]	519.5
0.25	6, [11]	521.0
0.17	5, [13]	521.0
0.13	4, [10]	520.5

Table 5.4: Effect of hydrazine addition rate on particle size and λ_{max}. Conditions: [$HAuCl_4$]: 0.1 M; [N_2H_5OH]: 1.0 M; [AOT]: 0.1 M; Temperature: 24 ± 1 °C. "**λ_{max}**" refers to the SPR absorbance peak in the UV-visible spectra.

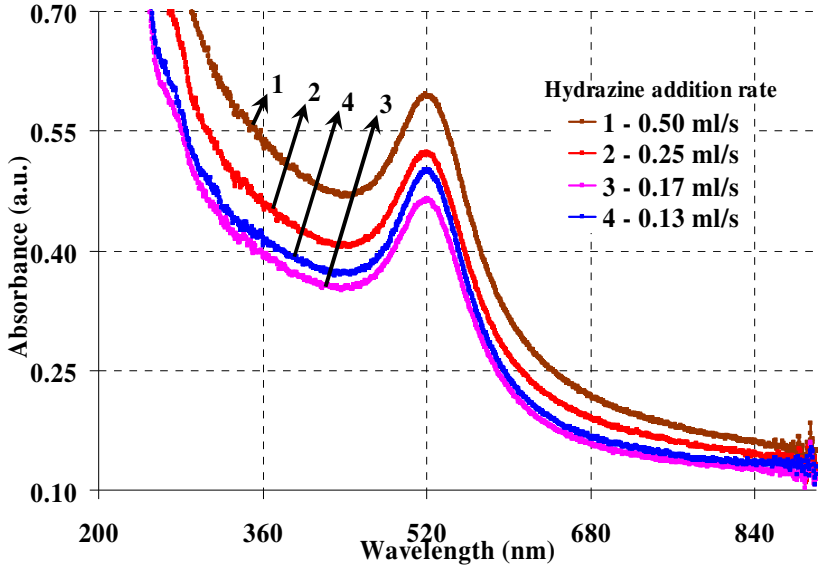

Fig. 5.4: UV-visible spectra of gold nanoparticles synthesized at various addition rates. Conditions: [$HAuCl_4$]: 0.1 M; [N_2H_5OH]: 1.0 M; [AOT]: 0.1 M.

The particle size was found to be around 5 nm, which is in accord with the reported value of 4.2 ± 1.0 nm (W_o= 6) [9]. The effect of addition rate of reducing agent on particle size was found to be insignificant. Chiang [7] has reported that the particle size is bigger in the presence of Brij 30 than in its absence while Surya [10] has reported that particle size was smaller in the presence of co-surfactant. From the current work, it can be inferred that the average particle size is bigger in the presence of co-surfactant.

However, the particles were not stable for more than 4 weeks. Particles agglomerated and settled as a dark precipitate at the bottom of the sample cell. Further, It was decided to increase the concentration of AOT to 0.2 M to check if this improved the stability of the synthesized nanoparticles. In this case, 10 ml of hydrazine micellar solution was added to 10 ml gold chloride micellar solution, in less than 5 seconds using a 60 ml separating funnel. The above experiment was carried at two different temperatures; 25 ± 1 °C and 30 ± 1 °C. At high temperature (~30°C), the particle size was found to be 4.5 ± 0.9 with percent polydispersity having a value of 6 while at the lower temperature (~25°C), the particle size was 7.3 ± 1.7 with 10 % polydispersity. The area under the SPR peak between 400 nm to 650 nm was 3 (a.u.) and 16 (a.u.) at 30 °C and 25 °C respectively. This shows that this system is not a potential option for

synthesizing nanoparticles at higher temperatures. The increase in the nanoparticle size with increase in AOT concentration can be attributed to the fact that the micellar fusion may be hindered due to an increase in the AOT concentration [11]. Furthermore, the interface becomes more rigid with increase in the AOT concentration, which is a critical parameter that affects the stability of nanoparticles in solution.

5.4 Gold nanoparticle synthesis in quaternary system

Based on the reverse micelle study, Brij 30 was included in the system to enhance the reverse micellar fusion process. The concentration of Brij 30 was kept at 0.1 M so as to maintain the molar ratio of co-surfactant to surfactant at 0.5. Now with the changed parameters (0.1 M Brij 30, 0.2 M AOT and molar ratio of water to AOT is 8), nanoparticles were synthesized by injecting 10 ml hydrazine reverse micellar solution to 10 ml gold chloride reverse micellar solution, in less than 5 seconds, using 60 ml separating funnel. The concentration of gold chloride and hydrazine was 0.05 M and 0.5 M respectively. The temperature was 31 ± 1 °C. The size of the particles was found to be 6.0 ± 0.3 with 5 % polydispersity based on DLS. The area under the SPR peak in the UV-visible spectra was found to be 30 (a.u.), which is at least 100 % more than the experiments performed without Brij 30. Also, it is to be noted that this experiment was carried at 31 ± 1 °C, which shows the robustness of this system with respect to reaction temperature. Hence, this system was chosen for studying the effects of parameters like temperature, reagent addition rate and concentration on particle size and its distribution.

5.4.1 Effect of mixing volume

Two different experiments were carried out by changing the total volume of reactants. The results of these experiments are summarized in the Table 5.5. This result is in accord with the one reported in Table 4.2. Both yield and polydispersity vary significantly upon scaling up. This is attributed to the use of magnetic stirrer for mixing. With increase in total volume of reactants, there is a possibility of increasing the dead-zone, which can help in explaining the increase in percentage polydispersity with increase in total volume of reactants. Also, the qualitative yields are not similar.

Total volume of reactants (ml)	Size (nm)	% Polydispersity	Area under SPR
20	6.0 ± 0.3	5	30
40	4.6 ± 0.4	20	41

Table 5.5: DLS characterization on the effect of total volume of reactants on particle size and its distribution along with area under the SPR in the UV-visible spectra. Conditions: [AOT]: 0.2 M; [Brij 30]: 0.1 M; Molar ratio of water to AOT is 8; Mixing system: Magnetic stirrer. "%Polydispersity" refers to the percentage variation of standard deviation with respect to mean particle size.

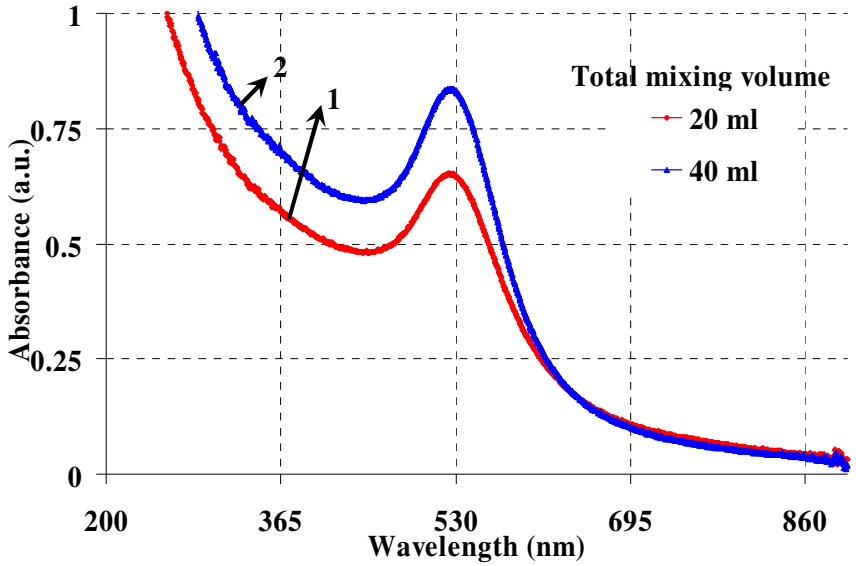

Fig. 5.5: UV-visible spectra of gold nanoparticles synthesized at different reaction volumes. Conditions: [AOT]: 0.2 M; [Brij 30]: 0.1 M; Molar ratio of water to AOT is 8; Mixing system: Magnetic stirrer.

5.5 Conclusions

The main objective of the systematic reverse micelle study was to develop a robust protocol, which is reproducible and repeatable, for synthesizing gold nanoparticles. For achieving reproducible results using microemulsions, they have to be prepared in a similar way. Sonication process helps in attaining reproducible dispersion of surfactants. Further, the sonication time is found to be a crucial parameter for reducing the polydispersity of droplets. It was found that a minimum of 15 minutes is required for AOT-isooctane system. The issues related with DLS measurement of micelle size and Wo values reported in literature were also resolved. The need for co-surfactant, Brij 30 is

explained from a structural perspective that suggests the appropriate concentration of co-surfactant. This was further validated with both DLS measurements of reverse micelle size and nanoparticle size, and feasible operating conditions to synthesize stable gold nanoparticles were also established. The issues related with limitations in scaling up of the system based on mixing using magnetic stirrers were also highlighted.

5.6 References

[1]. P. D. I. Fletcher, A. M. Howe and B. H. Robinson, 'The kinetics of solubilisate exchange between water droplets of a water-in-oil microemulsion', Journal of Chemical Society Faraday Transactions, 1, 83, 1987, pp. 985-1006.

[2]. M. Zulauf and H. F. Eicke, 'Inverted micelles and microemulsions in the ternary system H_2O/Aerosol-OT/Isooctane as studied by photon correlation spectroscopy', The Journal of Physical Chemistry, 83, 4, 1979, pp. 480-486.

[3]. L. M. M. Nazario, T. A. Hatton, and J. P. S. G. Crespo, 'Nonionic cosurfactants in AOT reversed micelles: Effect on percolation, size and solubilization site', Langmuir, 12, 1996, pp. 6326-6335.

[4]. K. Landfester, N. Bechthold, F. Tiarks and M. Antonietti, 'Formation and stability mechanisms of polymerizable miniemulsions', Macromolecules, 32, 1999, pp. 5222-5228.

[5]. L. M. M. Nazario, J. P. S. G. Crespo, J. F. Holzwarth and T. A. Hattton, 'Dynamics of AOT and AOT/nonionic cosurfactant microemulsions: An Iodine-Laser temperature jump study', Langmuir, 16, 2000, pp. 5892-5899.

[6]. L. M. Prince, 'Microemulsions: Theory and Practice', Academic press, 1977, pp.137-138.

[7]. J. G. Darab, D. M. Pfund, J. L. Fulton, J. C. Linehan, M. Capel and Y. Ma, 'Characterization of a water in oil microemulsion containing a concentrated ammonium ferric sulfate aqueous phase', Langmuir, 10, 1994, pp. 135-141.

[8]. C. L. Chiang, 'Controlled growth of gold nanoparticles in AOT/$C_{12}E_4$/Isooctane mixed reverse micelles', Journal of Colloid and Interface Science, 239, 2001, pp.334–341.

[9]. M. L. Wu, D. H. Chen and T. C. Huang, 'Preparation of Au/Pt bimetallic nanoparticles in water-in-oil microemulsions', Chemical Materials, 13, 2001, pp. 599-606.

[10]. D. Surya, 'Synthesis and characterization of gold nanoparticles', Master of Engineering report, Indian Institute of Science, 2006.

[11]. H. B. Bohidar, M. Behboudnia, 'Characterization of reverse micelles by Dynamic Light Scattering', Colloids and Surfaces A: Physicochemical and Engineering Aspects, 178, 2001, pp. 313-323.

Chapter 6

Parametric study

There is a pressing need for developing lab-scale recipes for the synthesis of nanoparticles to industrial scale [1]. After establishing robust protocols for the synthesis of gold nanoparticles at the lab-scale and upon understanding the deleterious effects of mixing patterns on reproducibility, we desired to study the effects of engineering parameters like temperature and reagent addition rate in an experimental set-up that could be easily scaled up. The design and fabrication of an appropriate reactor set-up is explained in the following section. This is followed by discussions of the various parametric studies carried out to synthesize gold nanoparticles using the optimized protocols developed earlier.

6.1 Design and fabrication of impeller

In view of simulating industrial scale reactors, it was decided to design and fabricate impeller and baffles (made of Teflon) geometrically similar to those used in the chemical process industries. A standard 4-blade Rushton impeller was made along with 4-legged baffle as shown in the Figure 6.1.

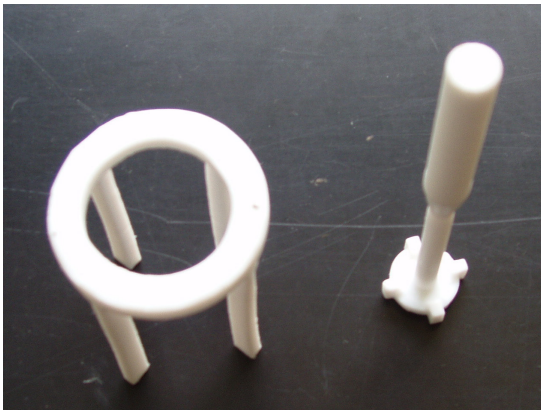

Fig. 6.1: Digital image of standard four-blade Rushton impeller and baffle made of Teflon

The parameters of the stirrer and the baffle are presented in Appendix 4. These were designed to fit in a standard 100 ml beaker, and the system can be scaled up easily to produce similar mixing patterns. The speed of the impeller was varied using a DC motor, which can maintain the same speed, irrespective of the volume of the reactants.

6.2 Effect of mixing volume

In view of examining the modified system, three experiments were carried out as shown in the Table 6.1. The concentrations of the reactants and surfactants used were similar to the experiment discussed in the section 5.4.1.

Run number	Total volume of reactants (ml)	Size (nm)	% Polydispersity	Area under SPR
1	20	5.8 ± 1.0	21	39
2	40	5.3 ± 0.3	17	34
3	40	7.6 ± 0.6	20	37

Table 6.1: Effect of total volume of reactants on particle size and its distribution and on the area under the SPR peak in the UV-visible spectra. Conditions: [AOT]: 0.2 M; [Brij 30]: 0.1 M; Water/AOT: 8; Mixing system: Rushton impeller along with baffles operated with DC motor operated at 750 rpm. "% Polydispersity" refers to the percentage variation of standard deviation with respect to mean particle size.

From the results, it can be inferred that the system is reproducible within experimental errors based on runs 2 and 3. The slight deviation in the size can be attributed to the variability of the point of injection of hydrazine reverse micellar solution to gold chloride using 60 ml separating funnel in those cases. The comparison of the results between run 1 and 2 showed that the particle size was not affected, which implies that the macroscale mixing was efficient at both conditions (i.e., with change in volume of reactants). Also, the UV-visible spectra for all three runs were similar as shown in Figure 6.2. This shows that the system is highly reproducible, and that optimized parameter ranges can be easily scaled up using dimension analysis arguments, as is routinely done in chemical process industry.

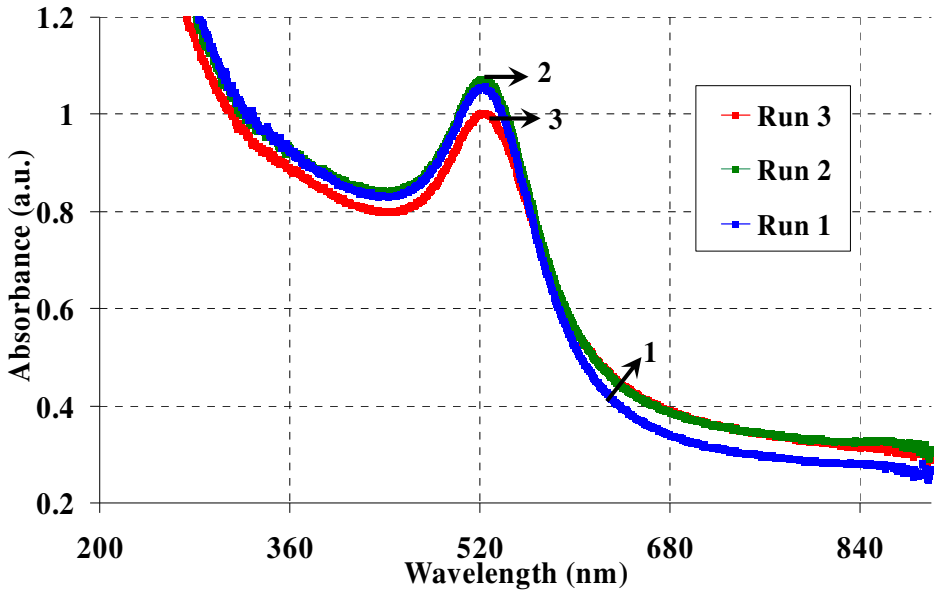

Fig. 6.2: UV-visible spectra of gold nanoparticles synthesized at different reaction volumes. Conditions: [AOT]: 0.2 M; [Brij 30]: 0.1 M; Water/AOT: 8; Mixing system: Rushton impeller along with baffles operated with DC motor operated at 750 rpm. Run 1, 2 and 3 refers to the reaction volumes of 20, 40 and 40 ml respectively.

6.3 Effect of mixing speed

A few experiments were performed to ensure that the choice of macroscopic mixing speed does not affect the particle size distribution. Based on intuition, it was thought that mixing speed would not play a role at high addition rates. In order to verify this, it was decided to carry out mixing speed study at two different addition rates (low and high), keeping all other conditions constant. The results of these experiments are tabulated in Table 6.2. The UV-visible spectra of the gold nanoparticles synthesized are shown in Figure 6.3.

Based on the results, it can be inferred that mixing speed does affect the quantity of stable nanoparticles, at low addition rates and does not affect this fraction at high addition rates. This is in line with the following hypothesis. At high hydrazine addition rates, the reduction of gold chloride ions occurs at a much faster timescale compared to the low addition rates. In the case of low addition rate, the nucleation overlaps with the growth process over longer timescales, as a result of which the nucleated atoms continue to grow. This is because growth process is energetically more favorable than nucleation, as there is no new phase formation. Beyond a certain point, the particles do not remain

stable in solution. However, the final nucleated atoms remain stable in solution because of non-availability of gold atoms to grow. Hence, the effect of mixing speed on particle size is insignificant.

Run number	Mixing speed (RPM)	Hydrazine addition rate (ml/s)	Size (nm)	% PD	Area under SPR
1	200 ± 10	1.00	9.3 ± 0.7	20	39
2	720 ± 10	1.00	7.5 ± 2.9	11	42
3	1200 ± 10	1.00	10.6 ± 1.3	16	43
4	720 ± 10	0.33	11.1 ± 1.4	23	5
5	1200 ± 10	0.33	10.3 ± 1.5	24	17

Table 6.2: DLS measurement of the effect of mixing speed and hydrazine addition rate on particle size and its distribution and the area under the SPR peak in the UV-visible spectra. Conditions: [AOT]: 0.2 M; [Brij 30]: 0.1 M; Water/AOT: 8; Mixing system: Rushton impeller along with baffles operated with DC motor. "% PD" refers to the percentage variation of standard deviation with respect to mean particle size.

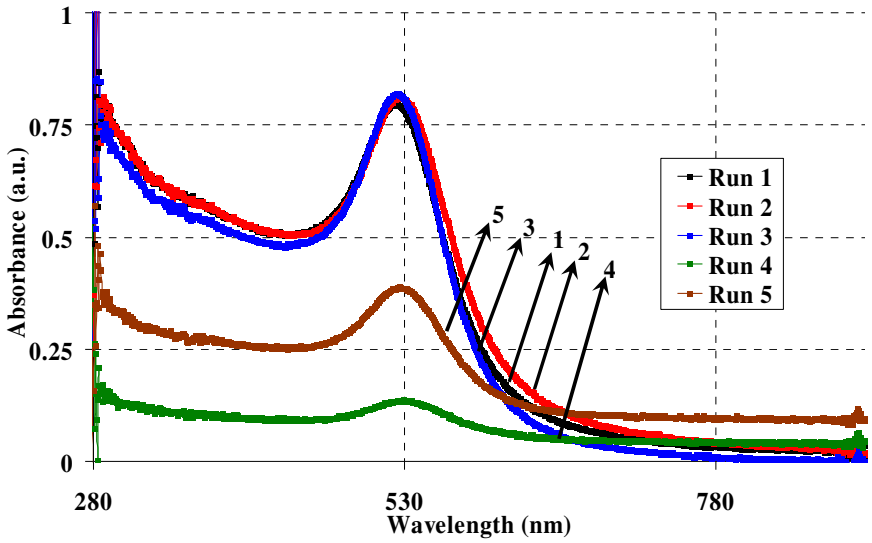

Fig. 6.3: UV-visible spectra of gold nanoparticles synthesized at different addition rates and mixing speed. Conditions: [AOT]: 0.2 M; [Brij 30]: 0.1 M; Water/AOT: 8; Mixing system: Rushton impeller along with baffles operated with DC motor. The notation of different runs can be found in Table 6.2.

It is seen that at high mixing speed, the yield of stable nanoparticles increases. Hence, the mixing speed could be decided based on the motor capacity and energy considerations. However, the problem with very high mixing speed is that it results in froth formation. This is undesirable for nanoparticle synthesis at the industrial scale. Thus, based on these two conflicting requirements, mixing speed of 750 rpm was chosen for nanoparticle synthesis, so as to synthesize nanoparticles in a reproducible manner.

6.4 Parametric study

The three steps involved during synthesis of metal nanoparticles are reduction of metal ions to atoms followed by nucleation and growth [2]. In the case of synthesis using microemulsions, these processes are believed to occur within reverse micelles even though there is discrepancy between initial reverse micelle size and final particle size. As microemulsions are self-assembled aggregates, whose properties depend on parameters like temperature, surfactant concentration, molar ratio of water to surfactant etc. and these parameters can be exploited to control particle size and its distribution. Nanoparticles are formed after numerous micellar collisions containing reactant species followed by reduction, nucleation and growth. The system temperature affects both micelle collision and reduction rates. Also, by varying the addition rate, the reduction process is presumed to be delayed, which further affects the relative rates of nucleation and growth processes. A few experiments were conducted to understand the effects of engineering parameters like temperature, hydrazine addition rate on particle size and its distribution. The results of these experiments are discussed below.

6.4.1 Effect of hydrazine addition rate and temperature

In the literature, only few groups have studied the effect of engineering parameters like reactant addition rate, temperature etc. on particle size and distribution. In the case of microemulsion mediated synthesis, only two groups have studied the effect of addition rate [3, 4]. The effect of temperature on reverse micelles has been studied by many groups. However, the effect of temperature on nanoparticle size has not been studied. This is a crucial parameter during the large scale production of nanoparticles. Schmidt et al. have prepared palladium nanoparticles using nonionic microemulsions [3].

They have studied the effect of mixing speed and reactant feed rate on particle size and its distribution. They have reported the both the effect of mixing speed and reactant feed rate on particle size distribution is only minor. However, they observed a decrease in the polydispersity when the precursor salt was injected instead of reducing agent reverse micellar solution. Adityawarman and his co-workers have synthesized $BaSO_4$ nanoparticles using non-ionic microemulsions [4]. They have examined various parameters like feeding rate, stirring rate, feeding sequence, and reactant concentration etc. on particle size distribution. They have reported that only the reactant concentration has an effect on particle size and its distribution. Even then, they believe that the effect of feeding rate and other parameters will be more pronounced at the production of nanoparticles at large scale.

The fusion efficiency of reverse micelles increases with an increase in temperature [5]. It is reported to double for a variation of temperature from 25 to 30 °C. Further, the phase diagram of water-AOT-isooctane changes drastically below 18 °C i.e. the solubility of water in AOT/isooctane decreases resulting in macroemulsions [6]. Hence, the temperature was varied in the range of 20-30 °C.

The previously optimized synthesis protocol and processing conditions were used. Briefly, the concentration of gold chloride and hydrazine hydrate was chosen as 0.05 and 0.5 M respectively. The concentrations of AOT and Brij 30 were 0.2 and 0.1 M respectively. The molar ratio of water to AOT is 8. The mixing time and speed was fixed at 25 minutes and 740 ± 20 rpm. Gold nanoparticles were synthesized at eight different hydrazine addition rates along with three reaction temperatures. The entire study was repeated three times on different days so as to avoid any bias during preparation. Further, the temperature and hydrazine addition rate for synthesizing nanoparticles was chosen randomly. From glassware cleaning to sample characterization, everything was carried on the same day to avoid source variability. For each sample, DLS measurement was repeated six times. Thus, at particular addition rate and temperature, the particle size is averaged over eighteen measurements. However, in some cases, all eighteen measurements were not possible due to nuances related with characterization and/or synthesis. Nevertheless, in all cases, a minimum of ten measurements have been made. The difference in the number of measurements is negated while calculating standard error, as it depends on degrees of freedom.

6.4.1.1 Particle size and its distribution

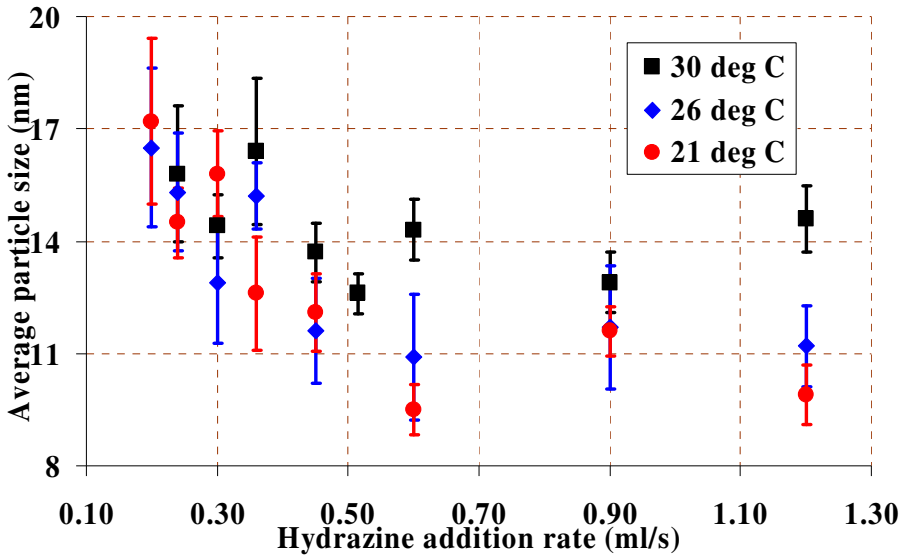

Fig. 6.4: DLS results for nanoparticle synthesis experiments conducted at different temperatures by varying the hydrazine addition rate. The error bars represent the standard error with 95 % confidence limit. The temperature variation is ± 1 °C.

Figure 6.4 represents the results of DLS measurements for nanoparticle synthesis experiments conducted at different temperatures by varying the hydrazine addition rate. Depending on the system temperature, different trends of hydrazine addition rate versus average particle size were observed. At the lower temperature (~21 °C), the average particle size increases from 9.9 ± 0.8 nm to 17.2 ± 2.2 nm (standard error with 95 % confidence limit) as the hydrazine addition rate decreases from 1.20 ml/s to 0.24 ml/s, while at higher temperature (~ 30 °C), particle size remained constant at 15 nm irrespective of the change in addition rate from 1.20 ml/s to 0.20 ml/s. However, at intermediate temperature (~ 26 °C), two different effects of addition rate on particle size was observed. Firstly, as the addition rate was varied from 1.20 ml/s to 0.45 ml/s, the particle size remained constant around 11 nm; upon further decrease in addition rate from 0.45 ml/s to 0.20 ml/s, the average particle size was found to increase from 11.6 ± 1.4 nm to 16.5 ± 2.1 nm (standard error with 95 % confidence limit). From the results, it can be seen that the maximum average particle size obtained in this system is around 17 nm, irrespective of temperature. Depending on the operating temperature, this value is achieved at high or low hydrazine addition rate. With increase in temperature, the value

of hydrazine addition rate at which the maximum particle size occurs increases. At low temperature (~21 °C), the value is at 0.20 ml/s while at high temperature it is 1.20 ml/s. Further, at a high hydrazine addition rate (1.20 ml/s), the average particle sizes are 9.9 ± 0.8, 11.2 ± 1.1 and 14.6 ± 0.9 nm at operating temperatures of 21, 26 and 30 °C respectively while at the lower addition rate (0.24 ml/s), the particle sizes are found to be 14.5 ± 0.9, 15.3 ± 1.6 and 15.8 ± 1.8 nm at 21, 26 and 30 °C respectively. This also indicates that the effect of hydrazine addition rate on particle size becomes more pronounced with decrease in temperature. This can be attributed to an increase in micellar fusion efficiency with increase in temperature. Thus, to tune the particle size with addition rate, operating temperature has to be lowered.

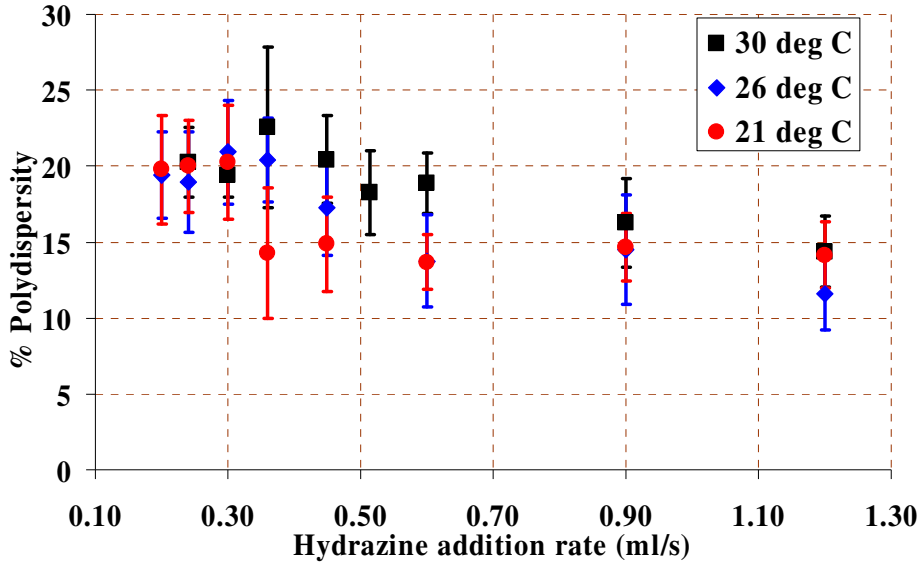

Fig. 6.5: Effect of hydrazine addition rate and temperature on polydispersity. The error bars represent the variation of mean size with 95 % confidence limit (Degrees of freedom: 15). The temperature variation is ± 1 °C.

Figure 6.5 represents the variation of polydispersity of the various samples synthesized at different addition rates and temperature. At 21 °C, the polydispersity decreased from 20 to 14 % as the addition rate was increased from 0.20 to 1.20 ml/s while at 26 °C, it varied from 19 to 12 %. However, at ~30 °C, the polydispersity was found to be constant at 20 % for all addition rates apart from the highest values of 0.90 and 1.20 ml/s, where the polydispersity was 16 and 14 % respectively. For obtaining monodisperse particles (< 5 % polydispersity), nucleation and growth must occur

independently [7]. In other words, nucleation must be instantaneous as it facilitates all the nucleated atoms to grow at same rate. However, decreasing hydrazine addition rates allow nucleation to overlap with the growth process over longer time scales, resulting in increased polydispersity [7]. However, detailed modelling is needed to analyze these trends more accurately.

From these results, it can be inferred that with increase in hydrazine addition rate, the particle size decreases. This result contradicts the results of Adityawarman et al. The group has claimed that the effect of reagent addition rate ($BaCl_2$ and K_2SO_4) on particle size is insignificant [4].

6.4.1.2 Yield of gold nanoparticles

It was observed visually that there is a decrease in the intensity of the colloidal solution with an increase in temperature. The digital images of these solutions are presented in Appendix 1.

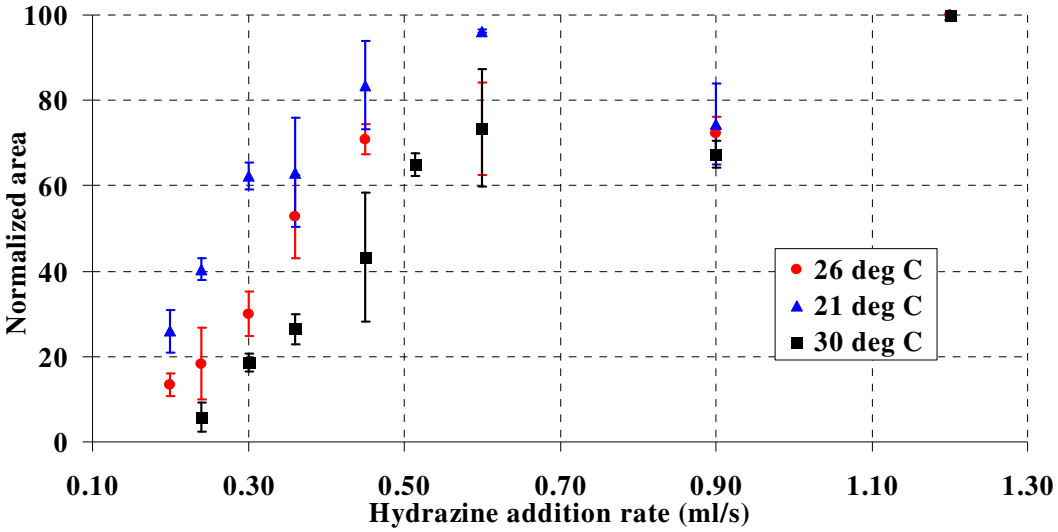

Fig. 6.6: Effect of hydrazine addition rate and temperature on the normalized area. "Normalized area" represents the area under the SPR peak in the UV-visible spectra normalized with the area obtained at highest hydrazine addition rate (1.20 ml/s). It is qualitative measure of yield of nanoparticles.

In order to quantify this effect, the area under the SPR peak in the UV-visible spectra between 400 to 650 nm was calculated for all the samples. The results are shown in Figure 6.6. It is found that with a decrease in hydrazine addition rate, the percentage

area normalized with the highest addition rate decreases irrespective of the temperature. However, the rate at which the area decays depends on the temperature. From this, it can be inferred that experiments cannot be carried out below certain addition rates depending on the temperature.

There was a clear transition in the color of colloidal solution from dark red to light pink at particular addition rate, which was found to be a function of temperature. The digital images of this observation are presented in Appendix 1. At low temperature, the transition occurred at 0.24 ml/s while for medium and high temperature it occurred at 0.30 and 0.45 ml/s respectively. From this, again it can be seen that micellar fusion increases with increase in temperature.

6.4.1.3 Color transition time

The initial gold chloride micellar solution is pale yellow in color. With the addition of reducing agent, the solution color changes from yellow to pink followed by deep red. The actual intensity of the colloidal gold solution depends on the operating conditions. The time taken for the onset of pink color was observed visually for samples synthesized at different hydrazine addition rates and temperatures. The onset of pink color is a probable indicator for the start of growth phase, as nuclei being smaller do not have a pronounced SPR. The results are presented in Figure 6.7

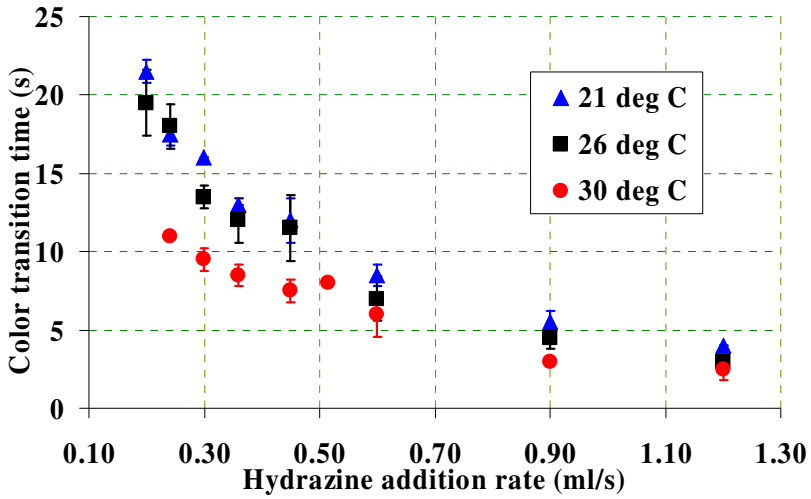

Fig. 6.7: Effect of hydrazine addition rate and temperature on color transition time. "Color transition time' represents the onset of pink color upon addition of hydrazine to the gold chloride reverse micellar solution.

Further, the amount of excess reducing agent required for color transition was calculated from color transition time. The amount of excess reducing agent (based on stochiometric requirements (Ref: Equation 1.1)) required for color transition was estimated to be 3.2 ± 0.3, 2.8 ± 0.3 and 2.1 ± 0.3 at 21, 26 and 30 °C respectively. These values are obtained visually and also based on two repetitions of eight addition rate experiments at a given temperature. These corroborate the fact that micellar fusion increases with increase in temperature.

6.5 Conclusions

A standard 4-blade Rushton impeller along with baffles, made of Teflon, were designed and fabricated. The design was validated, and the mixing patterns were found to be similar for different reaction volumes. Also, the effect of impeller speed was found to be significant only at low addition rates. It was found that with decrease in addition rate from 1.20 ml/s to 0.20 ml/s, both average particle size and polydispersity increases, irrespective of the reaction temperature. However, the range of increase of particle size depends on the temperature. The effect of hydrazine rate on particle size was found to be more pronounced at lower temperature. Further, similar trend of decrease in yield and stability of nanoparticles was observed. The rate of decrease of yield of stable nanoparticles increases with increase in temperature. This has been validated based on both color transition time and area under the SPR peak in the UV-visible spectra. Moreover, the normalized area under the SPR in the UV-visible spectra decreases with increase in hydrazine addition rate. The color transition time is a probable indicator for the start of growth phase.

6.6 References

[1]. D. L. Marchisio, L. Rivautella and A. A. Barresi, ‘Design and scale-up of chemical reactors for nanoparticle precipitation’, American Institute of Chemical Engineers Journal, 52, 5, 2006, pp. 1877-1887.

[2]. C. Baker, A. Pradhan and I. Shah, ‘Metal nanoparticles’, Encyclopedia of Nanoscience and Nanotechnology’, Vol.5, Edited by H. S. Nalwa, 2004, pp. 449-473.

[3]. J. Schmidt, C. Guesdon and R. Schomacker, ‘Engineering aspects of preparation

of nanocrystalline particles in microemulsions', Journal of Nanoparticle Research, 1, 1999, pp. 267-276.

[4]. D. Adityawarman, A. Voigt, P.Veit and K. Sundmacher, 'Precipitation of $BaSO^4$ nanoparticles in a non-ionic microemulsion: Identification of suitable control parameters', Chemical Engineering Science, 60, 2005, pp. 3373-3381.

[5]. P. D. I. Fletcher, A. M. Howe and B. H. Robinson, 'The kinetics of solubilisate exchange between water droplets of a water-in-oil microemulsion', Journal of the Chemical Society, Faraday Transactions, 1, 83, 1987, pp. 985-1006.

[6]. L. M. Prince, 'Microemulsions: Theory and Practice', Academic press, 1977, pp.1-145.

[7]. D. Kim, S. Jeong and J. Moon, 'Synthesis of silver nanoparticles using the polyol process and the influence of precursor injection', Nanotechnology, 17, 2006, pp. 4019-4024.

Chapter 7

Summary and recommendations

7.1 Summary

The main contributions of this project are summarized below

- A robust protocol, which is repeatable and reproducible, for synthesizing gold nanoparticles using microemulsions was developed.
    - The amount of reducing agent has to be 12 times in excess of the stochiometric requirement to form stable nanoparticles; this can be attributed to the possibility of side reaction between AOT and hydrazine
    - Higher amount of gold chloride concentration results in an increase in the stability of nanoparticles formed.
- The area under the Surface Plasmon Resonance (SPR) peak in the UV-visible spectra between 400 to 650 nm is found to be a valid indicator for quantifying yield and stability of gold nanoparticles in solution.
- DLS characterization on reverse micelles was performed and the major findings are listed below,
    - Sonication helps in reducing the polydispersity of reverse micelles and improves the reproducibility of experiments.
    - Sonication time is a critical parameter; a minimum of 15 minutes is needed for reducing the polydispersity of reverse micelles.
    - Sonication is needed at low molar ratio of water to AOT and not at higher ratios.
    - Brij 30 is the optimal choice as co-surfactant for water-AOT-isooctane system and helps in increasing micellar fusion as shown by the increased yield and stability of nanoparticles.
- A standard 4-blade Rushton impeller with four legged baffle has been designed and verified.

- The impeller speed is found to have an effect on particle size and yield only at low hydrazine addition rates.
- With increase in hydrazine addition rate, both particle size and polydispersity decreases.
- Depending on reaction temperature, different trends of hydrazine addition rate versus particle size was observed. At low temperature (21 ° C), with decrease in addition rate, the average particle size increased while at high temperature (30 °C), the particle size was found to be constant. Further, at intermediate temperature, both trends were observed.
- The yield of stable nanoparticles was found to decrease with decrease in hydrazine addition rate, irrespective of the temperature. However, with increase in temperature, the rate of decrease of yield of nanoparticles increased. This indicates that micellar fusion efficiency increases with increase in temperature. This was further validated with the color transition time (or amount of excess reducing agent). This is a probable indicator for the start of growth phase.

7.2 Recommendations for future work

Some of the unresolved issues are listed below,

- The maximum particle size obtained is a function of molar ratio of water to surfactant, which determines the initial reverse micelle size. However, the actual value of the nanoparticle size is not limited to the size of the reverse micelle. This aspect needs to be understood.
- Detailed modelling is required to understand the effect on particle size of parameters like temperature and addition rate of reactants on particle size.
- The kinetics of reactions within reverse micelles should be monitored using stopped flow reactor to help in modelling.
- More complicated systems like Fe-Pt need to be synthesized to further optimize the protocols.

Appendix 1: Digital images of gold nanoparticles

Fig. A1.1: Digital photograph of gold nanoparticles synthesized with 0.05 M gold chloride concentration. Conditions: [Hydrazine]: 0.5 M; [AOT]: 0.1 M; [Brij 30]: 0.2 M and molar ratio of water to AOT of 24. Arrows indicates the direction of decreasing hydrazine addition rate.

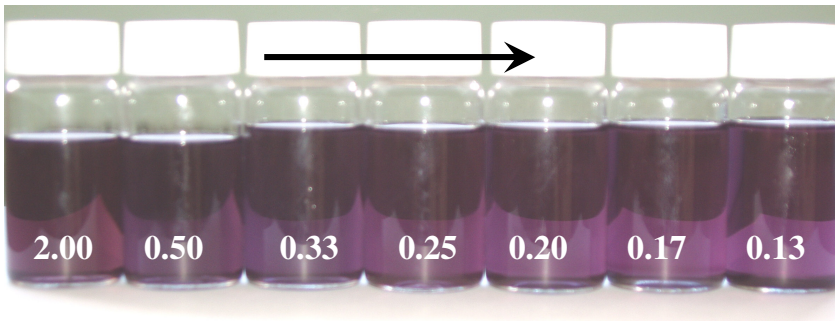

Fig. A1.2: Digital photograph of gold nanoparticles synthesized with 0.0125 M gold chloride concentration. Conditions: [Hydrazine]: 0.125 M; [AOT]: 0.1 M; [Brij 30]: 0.2 M and molar ratio of water to AOT of 24. Arrows indicates the direction of decreasing hydrazine addition rate.

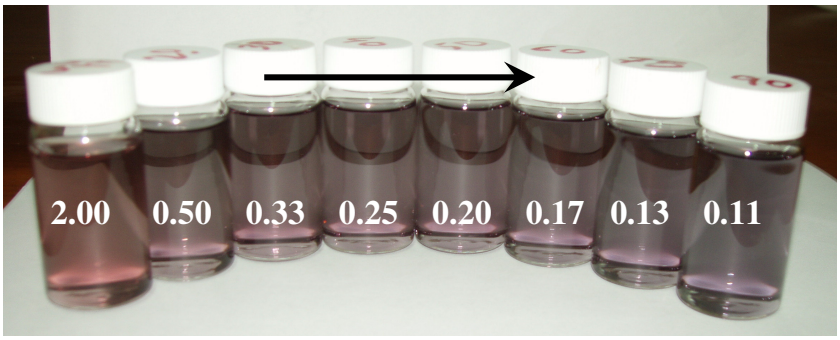

Fig. A1.3: Digital photograph of gold nanoparticles synthesized with 0.00625 M gold chloride concentration. Conditions: [Hydrazine]: 0.0625 M; [AOT]: 0.1 M; [Brij 30]: 0.2 M and molar ratio of water to AOT of 24. Arrows indicates the direction of decreasing hydrazine addition rate.

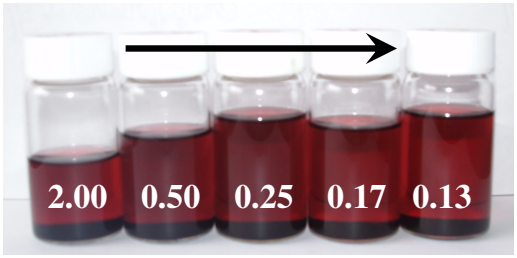

Fig. A1.4: Digital photograph of gold nanoparticles synthesized with 0.1 M gold chloride concentration. Conditions: [Hydrazine]: 1.0 M; [AOT]: 0.1 M and molar ratio of water to AOT of 8. Arrows indicates the direction of decreasing hydrazine addition rate.

Fig. A1.5: Digital photograph of gold nanoparticles synthesized with 0.05 M gold chloride concentration. Conditions: [Hydrazine]: 0.5 M; [AOT]: 0.2 M and molar ratio of water to AOT of 8. Left image refers to particle synthesized at 30 °C; Right image at 25 °C.

Fig. A1.6: Digital photograph of gold nanoparticles synthesized depicting the effect of mixing. Conditions: [Gold chloride]: 0.05 M; [Hydrazine]: 0.5 M; [AOT]: 0.2 M; [Brij 30]: 0.1 M and molar ratio of water to AOT of 8. Temperature: 31 °C. Detailed experimental protocol followed for each sample is explained in the section.

Fig. A1.7: Digital photograph of gold nanoparticles synthesized depicting the effect of mixing speed. Conditions: [Gold chloride]: 0.05 M; [Hydrazine]: 0.5 M; [AOT]: 0.2 M; [Brij 30]: 0.1 M and molar ratio of water to AOT of 8. Temperature: 30 °C.

Fig. A1.8: Digital photograph of gold nanoparticles synthesized at different temperatures and hydrazine addition rate. Arrow indicates the direction of decreasing addition rate. The numbers superimposed on the sample cells indicate the addition hydrazine rate in ml/s. The temperature corresponds to the solution temperature. Conditions: [AOT]: 0.2 M; [Brij 30]: 0.1 M; Molar ratio of water to AOT: 8;

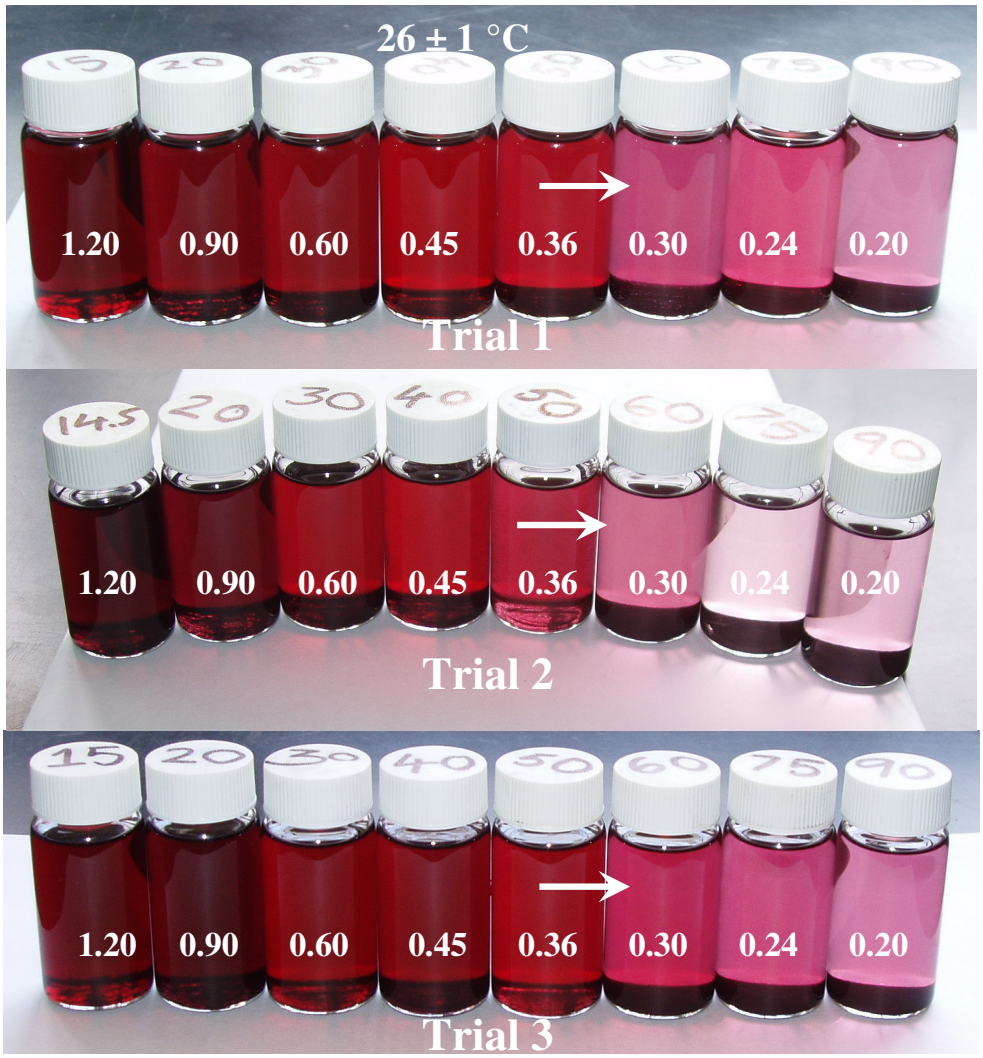

Fig. A1.9: Digital photograph of gold nanoparticles synthesized repeated three times at same temperature with different hydrazine addition rate. Arrow indicates the direction of decreasing addition rate. The numbers superimposed on the sample cells indicate the addition hydrazine rate in ml/s. The temperature corresponds to the solution temperature. Conditions: [AOT]: 0.2 M; [Brij 30]: 0.1 M; Molar ratio of water to AOT: 8;

Appendix 2: UV-visible spectra of gold nanoparticles

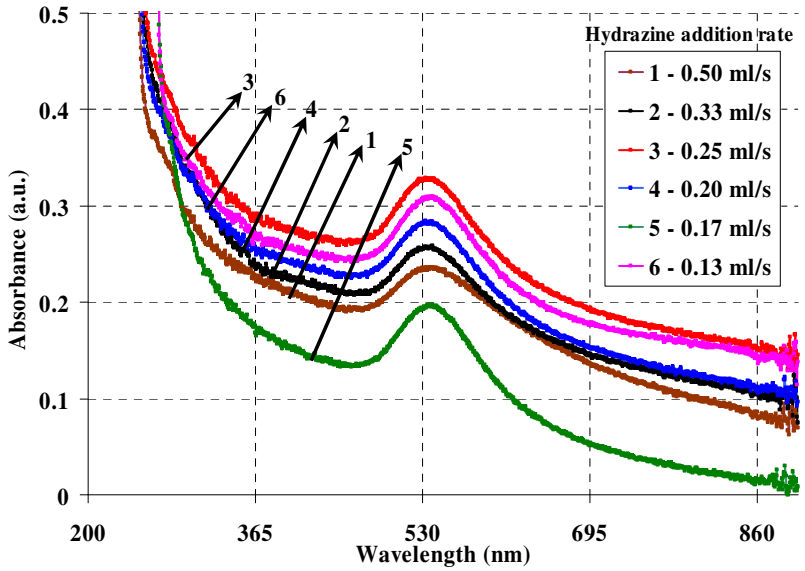

Fig. A2.1: UV-visible spectra of gold nanoparticles synthesized with the following conditions: [Gold chloride]: 0.0125 M; [Hydrazine]: 0. 125 M; [AOT]: 0.1 M; [Brij 30]: 0.2 M; Molar ratio of water to AOT: 24

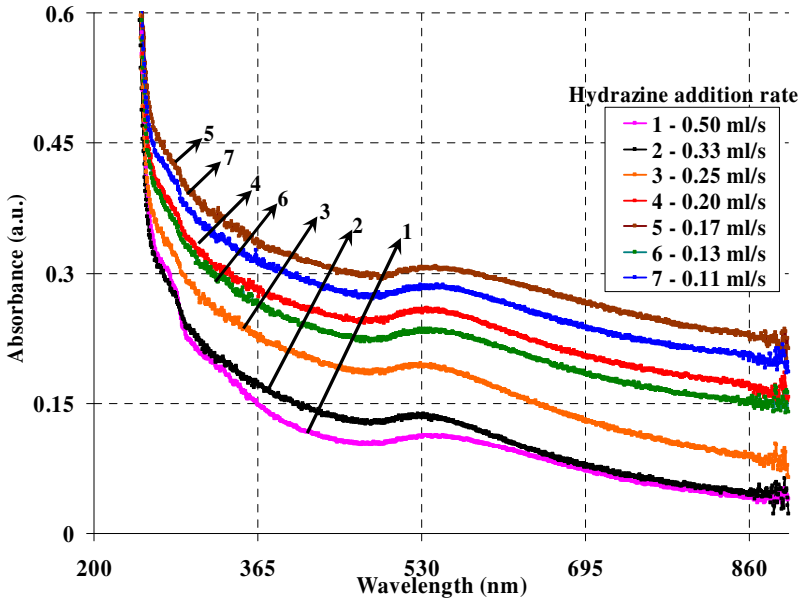

Fig. A2.2: UV-visible spectra of gold nanoparticles synthesized with the following conditions: [Gold chloride]: 0.00625 M; [Hydrazine]: 0. 0625 M; [AOT]: 0.1 M; [Brij 30]: 0.2 M; Molar ratio of water to AOT: 24

TEMPERATURE STUDY

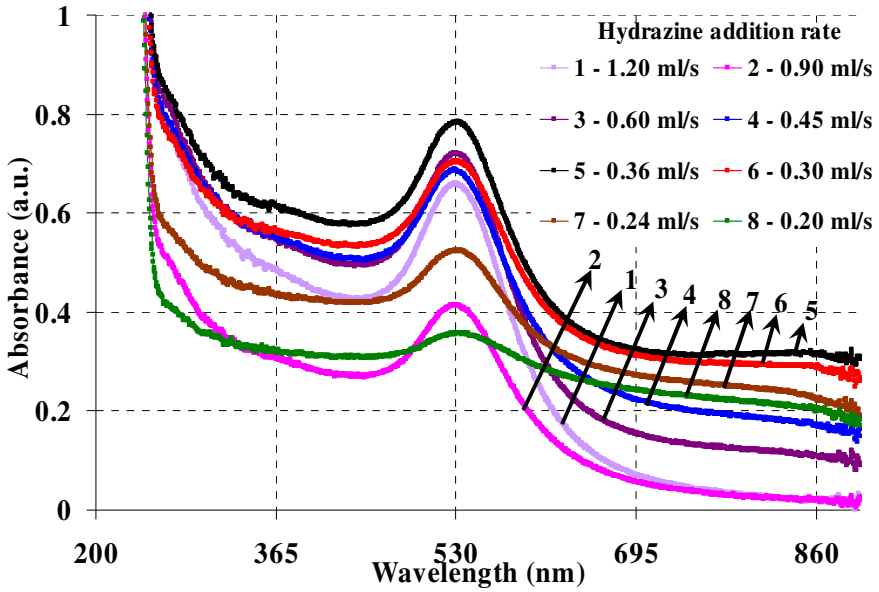

Fig. A2.3: UV-visible spectra of gold nanoparticles synthesized with various addition rates. Conditions: [Gold chloride]: 0.05 M; [Hydrazine]: 0. 5 M; [AOT]: 0.2 M; [Brij 30]: 0.1 M; Molar ratio of water to AOT: 8; Temperature: 21 ± 1°C

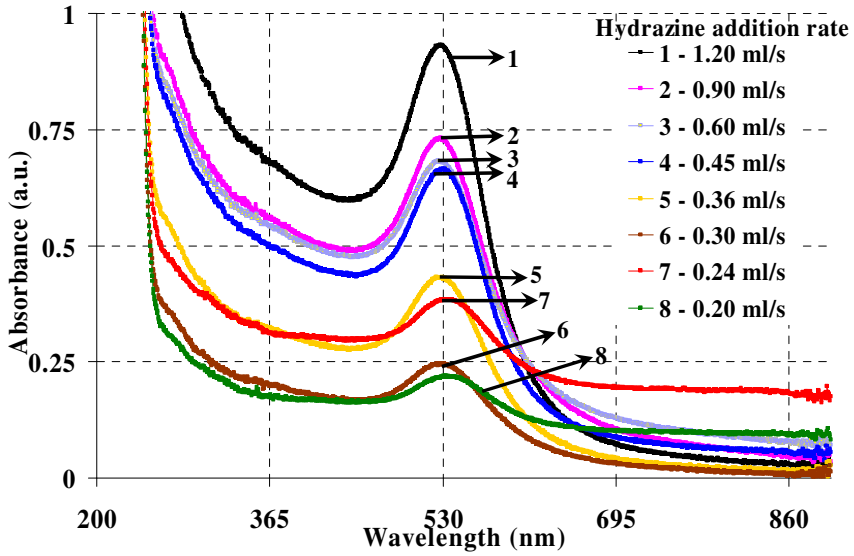

Fig. A2.4: UV-visible spectra of gold nanoparticles synthesized with various addition rates. Conditions: [Gold chloride]: 0.05 M; [Hydrazine]: 0. 5 M; [AOT]: 0.2 M; [Brij 30]: 0.1 M; Molar ratio of water to AOT: 8; Temperature: 26 ± 1°C

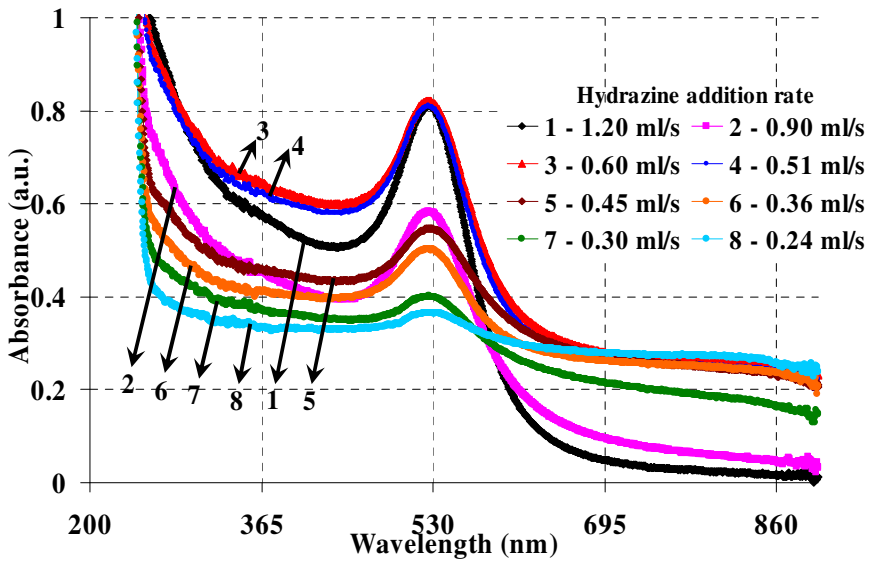

Fig. A2.5: UV-visible spectra of gold nanoparticles synthesized with various addition rates. Conditions: [Gold chloride]: 0.05 M; [Hydrazine]: 0. 5 M; [AOT]: 0.2 M; [Brij 30]: 0.1 M; Molar ratio of water to AOT: 8; Temperature: 30 ± 1°C

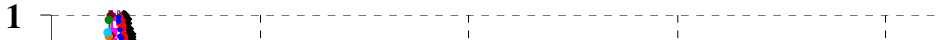

Appendix 3: TEM images of gold nanoparticles

SAMPLE 1

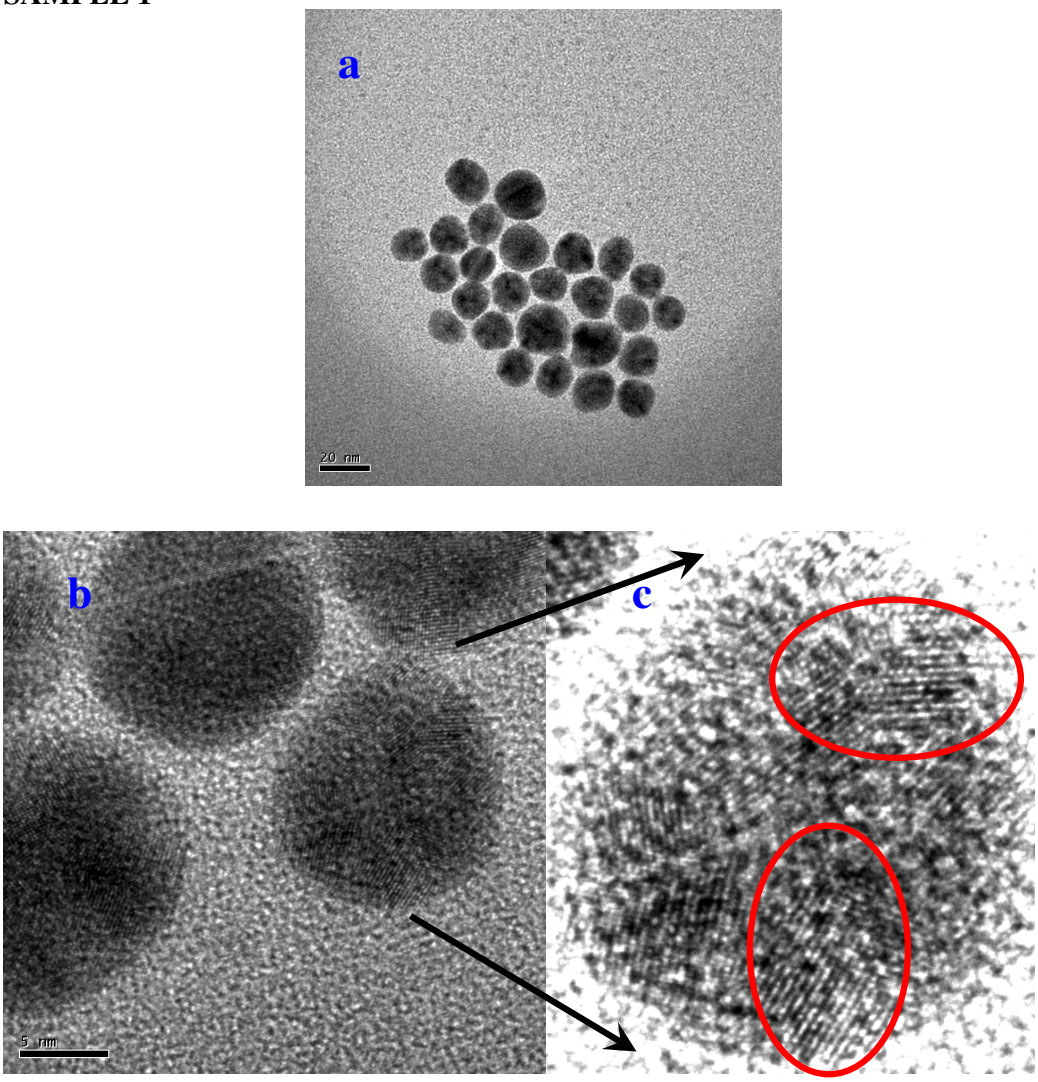

Fig. A3.1: Different magnifications of representative TEM images of gold nanoparticles; Scale bar for image a) 20 nm, b) 5 nm. Synthesis conditions: Concentrations of AOT and Brij 30 are 0.1 M and 0.2 M while the aqueous concentration of gold chloride and hydrazine are 0.05 M and 0.5 M respectively. The molar ratio of water to AOT was 24. The hydrazine addition rate was 0.50 ml/s. The two outlined regions (oval shaped) in the image 'c' are used to highlight the presence of lattice fringes. The distance between the lattice fringes in the vertical and horizontal oval region was found to be 0.236 and 0.201 nm, which can be indexed to planes {111} and {200}. This corroborates with well with the literature.

SAMPLE 2

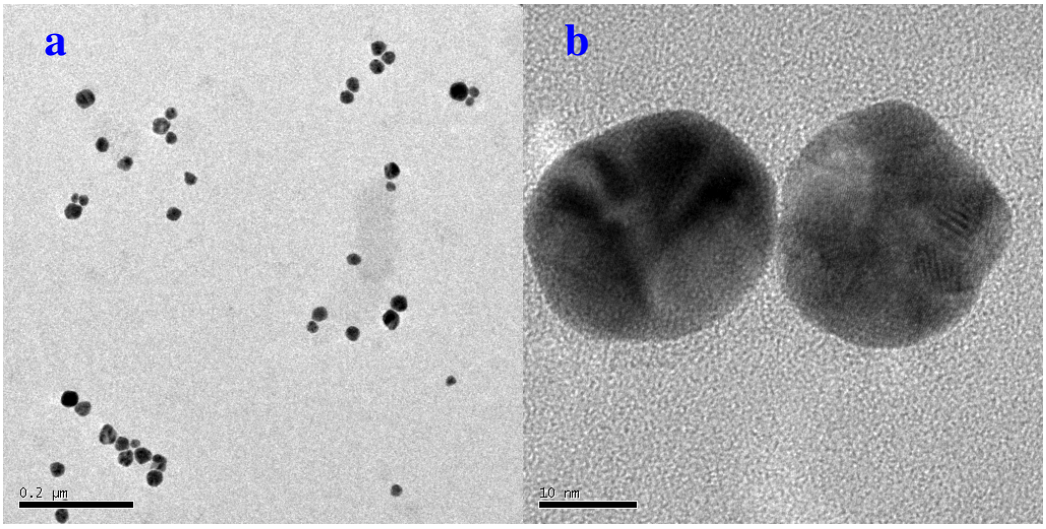

Fig A3. 2: Representative TEM images of gold nanoparticles with different magnifications. Scale bar for image a) 200 nm, b) 10 nm. Synthesis conditions: Concentrations of AOT and Brij 30 are 0.1 M and 0.2 M while the aqueous concentration of gold chloride and hydrazine are 0.05 M and 0.5 M respectively. The molar ratio of water to AOT was 8. The hydrazine addition rate was 0.25 ml/s.

SAMPLE 3 **SAMPLE 4**

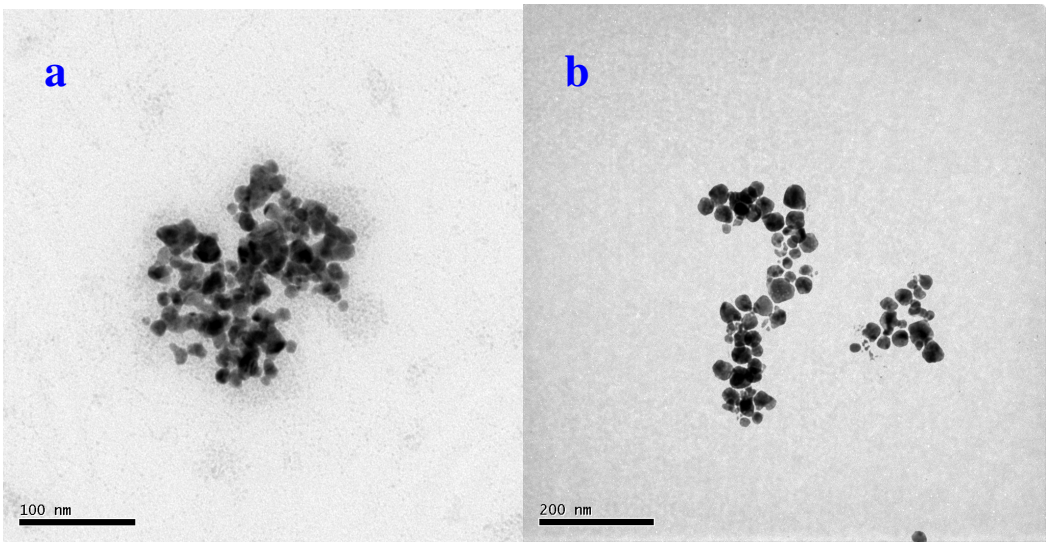

Fig A3. 3: Representative TEM images of gold nanoparticles. Scale bar for image a) 100 nm, b) 200 nm. Synthesis conditions: Concentrations of AOT and Brij 30 are 0.1 M and 0.2 M while the aqueous concentration of gold chloride and hydrazine are 0.0125 M and 0.125 M respectively. The molar ratio of water to AOT was 24. The hydrazine addition rate was a) 0.13 ml/s, b) 0.50 ml/s.

SAMPLE 5

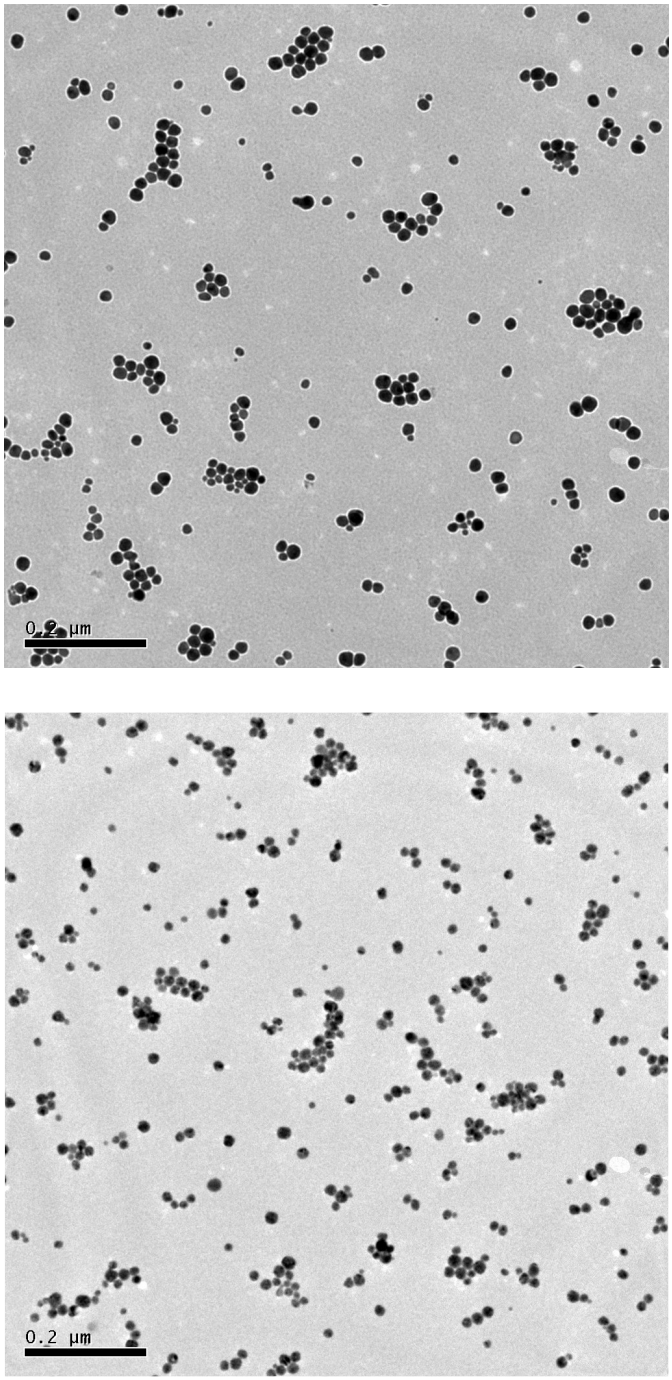

Fig A3. 4: Representative TEM images of gold nanoparticles imaged at two different locations on the same TEM grid. Scale bar: 200 nm. Synthesis conditions: Concentrations of AOT and Brij 30 are 0.2 M and 0.1 M while the aqueous concentration of gold chloride and hydrazine are 0.05 M and 0. 5 M respectively. The molar ratio of water to AOT was 8. The hydrazine addition rate was 1.20 ml/s and the operating temperature was 26 ± 1 °C.

SAMPLE 6

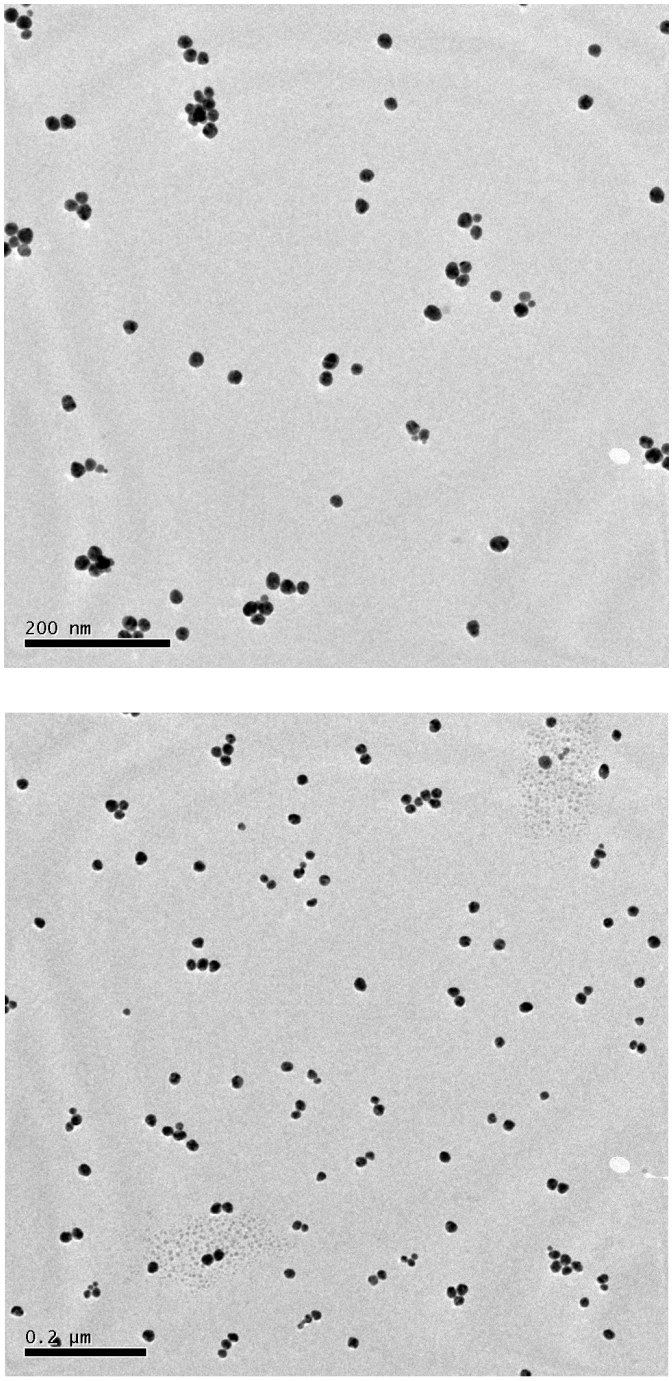

Fig A3. 5: Representative TEM images of gold nanoparticles imaged at two different locations on the same TEM grid. Scale bar: 200 nm. Synthesis conditions: Concentrations of AOT and Brij 30 are 0.2 M and 0.1 M while the aqueous concentration of gold chloride and hydrazine are 0.05 M and 0. 5 M respectively. The molar ratio of water to AOT was 8. The hydrazine addition rate was 0.45 ml/s and the operating temperature was 21 ± 1 °C.

SAMPLE 7

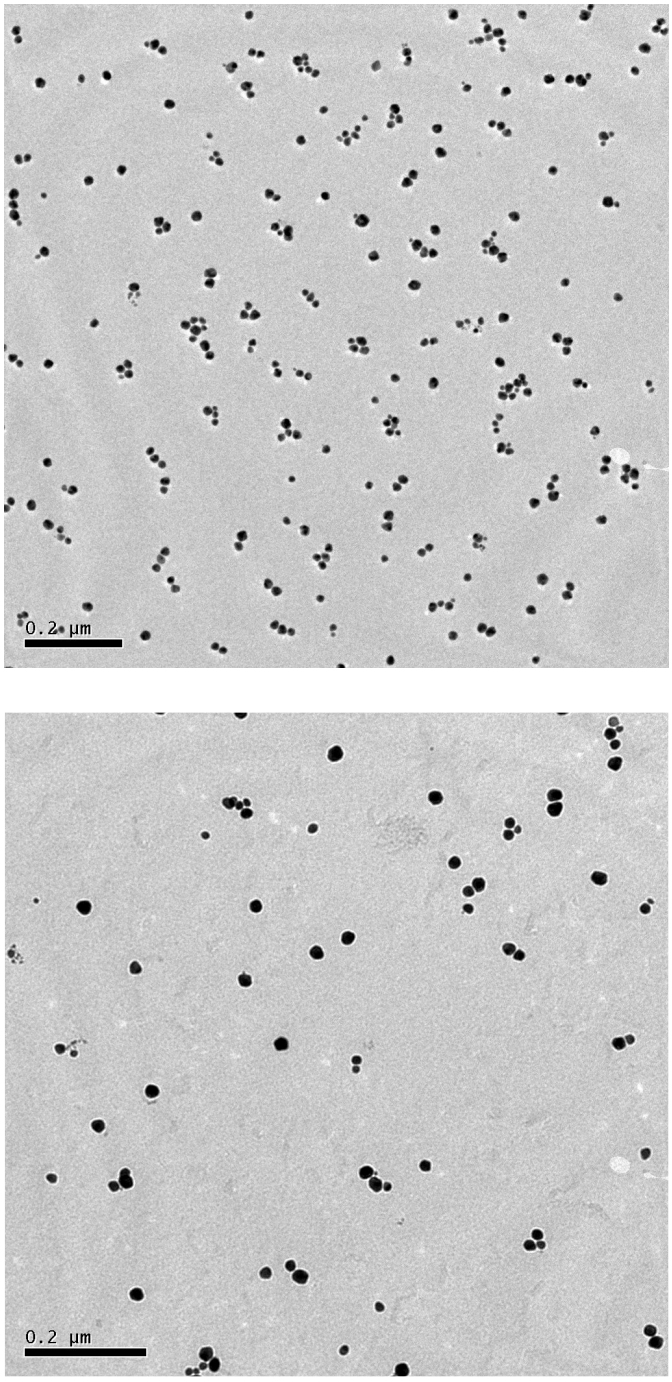

Fig A3. 6: Representative TEM images of gold nanoparticles imaged at two different locations on the same TEM grid. Scale bar: 200 nm. Synthesis conditions: Concentrations of AOT and Brij 30 are 0.2 M and 0.1 M while the aqueous concentration of gold chloride and hydrazine are 0.05 M and 0. 5 M respectively. The molar ratio of water to AOT was 8. The hydrazine addition rate was 0.45 ml/s and the operating temperature was 30 ± 1 °C.

SAMPLE 8

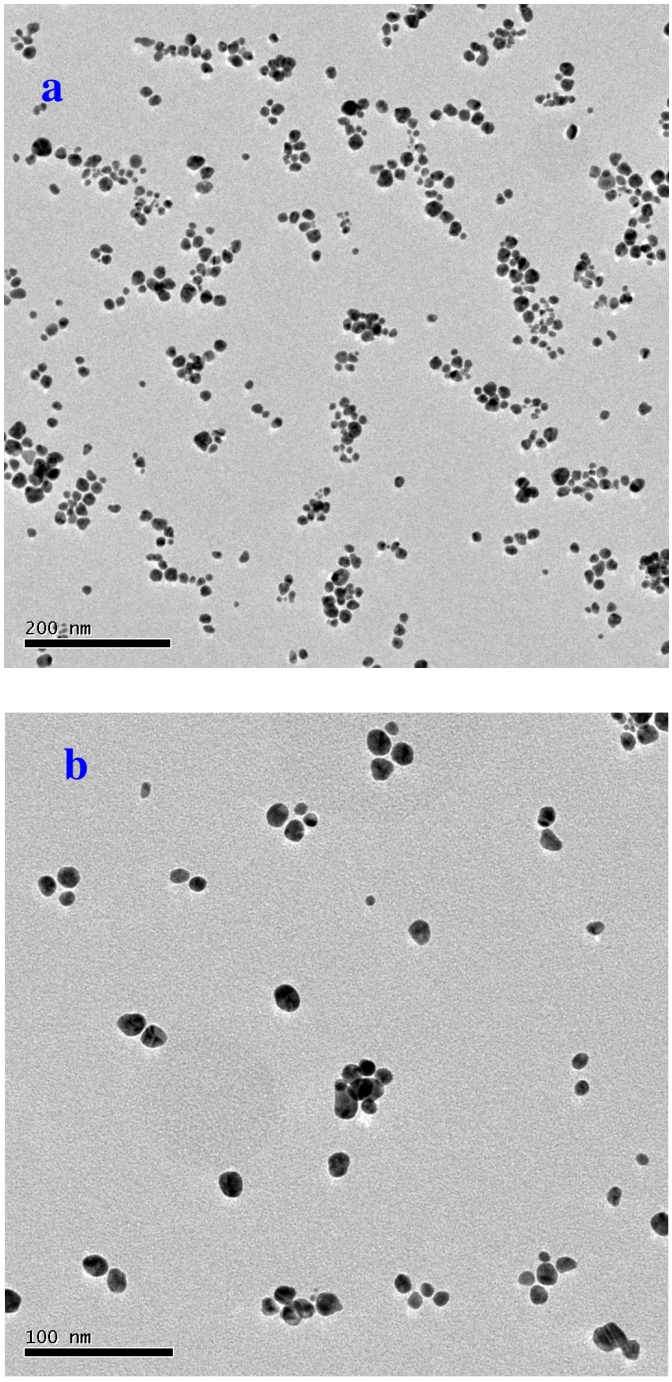

Fig A3. 7: Representative TEM images of gold nanoparticles with different magnifications. Scale bar for image a) 200 nm, b) 100 nm. Synthesis conditions: Concentrations of AOT and Brij 30 are 0.2 M and 0.1 M while the aqueous concentration of gold chloride and hydrazine are 0.05 M and 0. 5 M respectively. The molar ratio of water to AOT was 8. The hydrazine addition rate was 1.20 ml/s and the operating temperature was 21 ± 1 °C.

SAMPLE 9

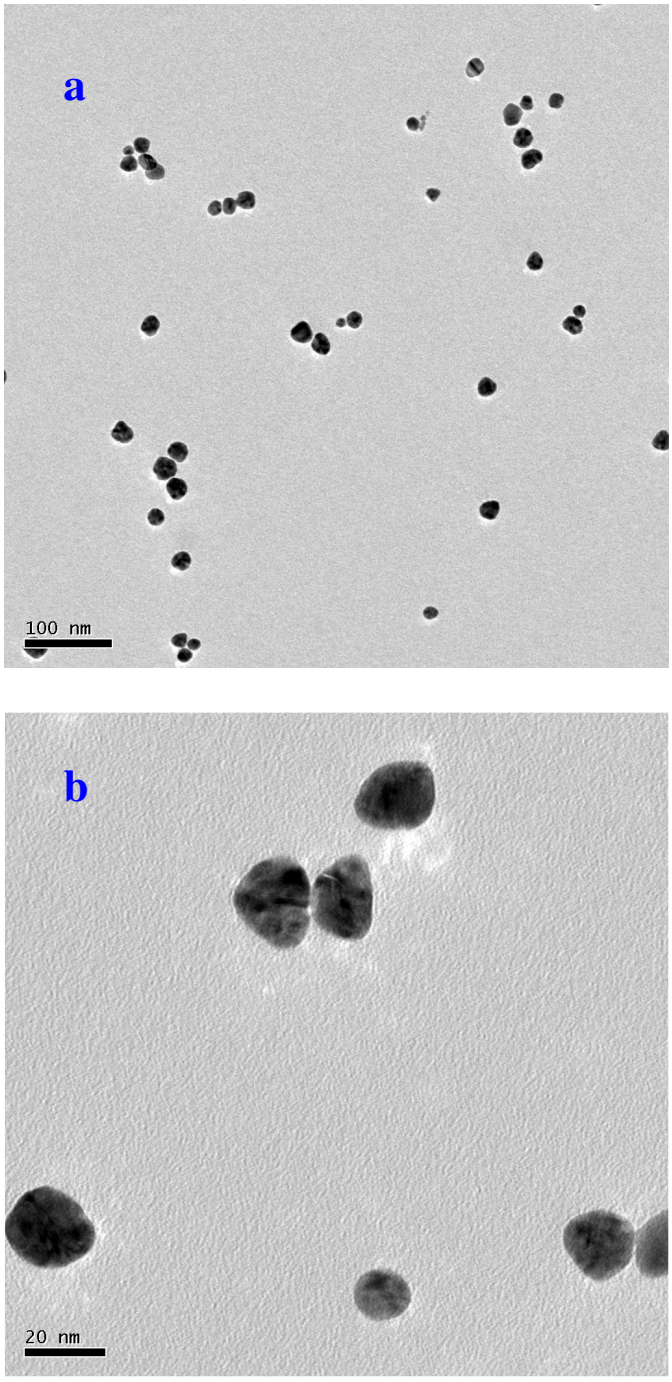

Fig A3. 8: Representative TEM images of gold nanoparticles with different magnifications. Scale bar for image a) 100 nm, b) 20 nm. Synthesis conditions: Concentrations of AOT and Brij 30 are 0.2 M and 0.1 M while the aqueous concentration of gold chloride and hydrazine are 0.05 M and 0. 5 M respectively. The molar ratio of water to AOT was 8. The hydrazine addition rate was 0.20 ml/s and the operating temperature was 21 ± 1 °C.

SAMPLE 10

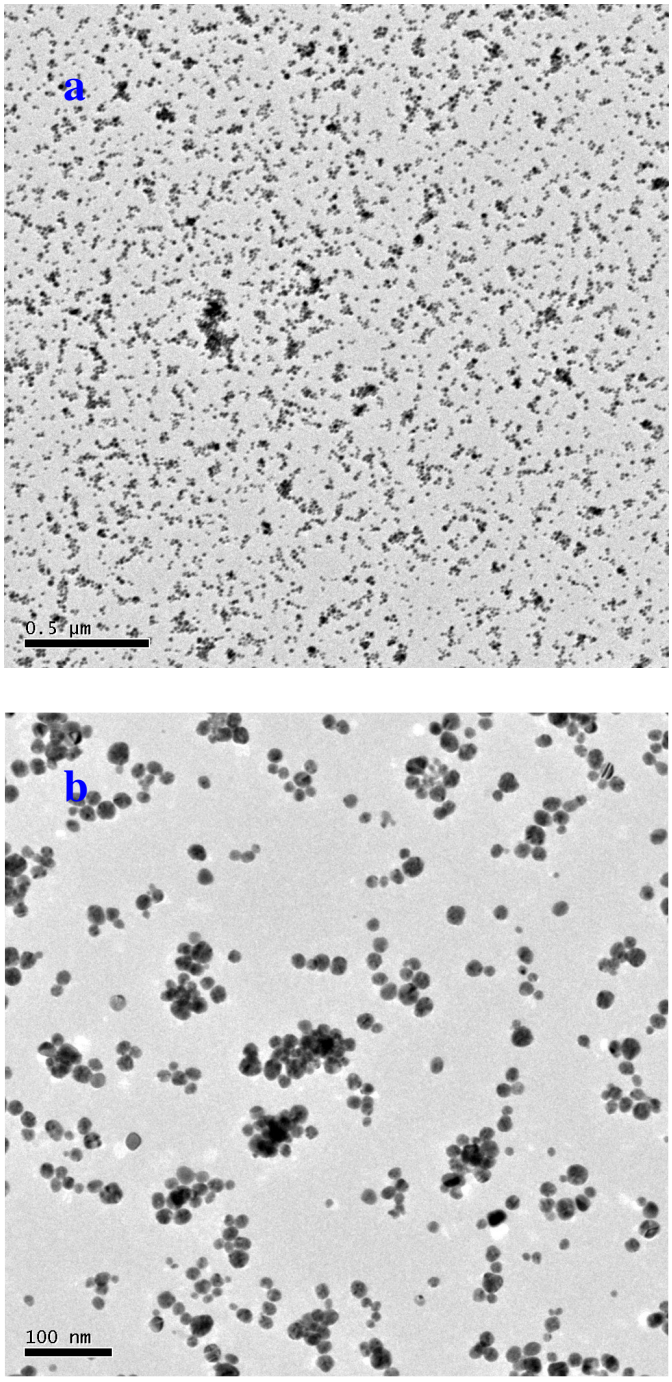

Fig A3. 9: Representative TEM images of gold nanoparticles with different magnifications. Scale bar for image a) 500 nm, b) 100 nm. Synthesis conditions: Concentrations of AOT and Brij 30 are 0.2 M and 0.1 M while the aqueous concentration of gold chloride and hydrazine are 0.05 M and 0. 5 M respectively. The molar ratio of water to AOT was 8. The hydrazine addition rate was 1.20 ml/s and the operating temperature was 30 ± 1 °C.

Sample number	Average particle size based on TEM (nm); [%PD]	Number of particles analyzed	Average particle size based on DLS (nm); [%PD]
1	16, [22]	46	11, [13]
2			
3	10, [32]	18	08, [12]
5	16, [30]	1410	11, [12]
6	17, [25]	823	12, [15]
7	17, [30]	863	14, [20]
8	15, [34]	1310	10, [14]
9	18, [30]	663	17, [20]
10	16, [33]	1299	15, [14]

Table A3.1: Comparison of TEM and DLS based on average particle size. The synthesis conditions for the respective samples are presented in the representative TEM images shown in this chapter. % PD refers to the percentage variation of standard deviation with respect to the average particle size. This was estimated from the pooled standard deviation.

The standard pooled deviation (σ_p) was calculated from the following formulae,

$$\sigma_p = \sqrt{\frac{(n_1-1)\sigma_1^{\,2} + (n_2-1)\sigma_2^{\,2} + \ldots + (n_k-1)\sigma_k^{\,2}}{n_1+n_2+\ldots+n_k-k}} \qquad \text{(A3.1)}$$

where n_k is the sample size of the k^{th} sample, σ_k is the standard deviation of the k^{th} sample and k is the number of samples coupled.

The TEM results indicate higher polydispersity as compared to DLS. The reason for this can be attributed to the less number of samples analyzed in TEM. Also, in most of the cases, the resolution (nm/pixel) of the TEM image was greater than 0.7. The images with resolution greater than 1.1 nm/pixel were not considered for TEM analysis.

Appendix 4: Impeller and baffle specifications

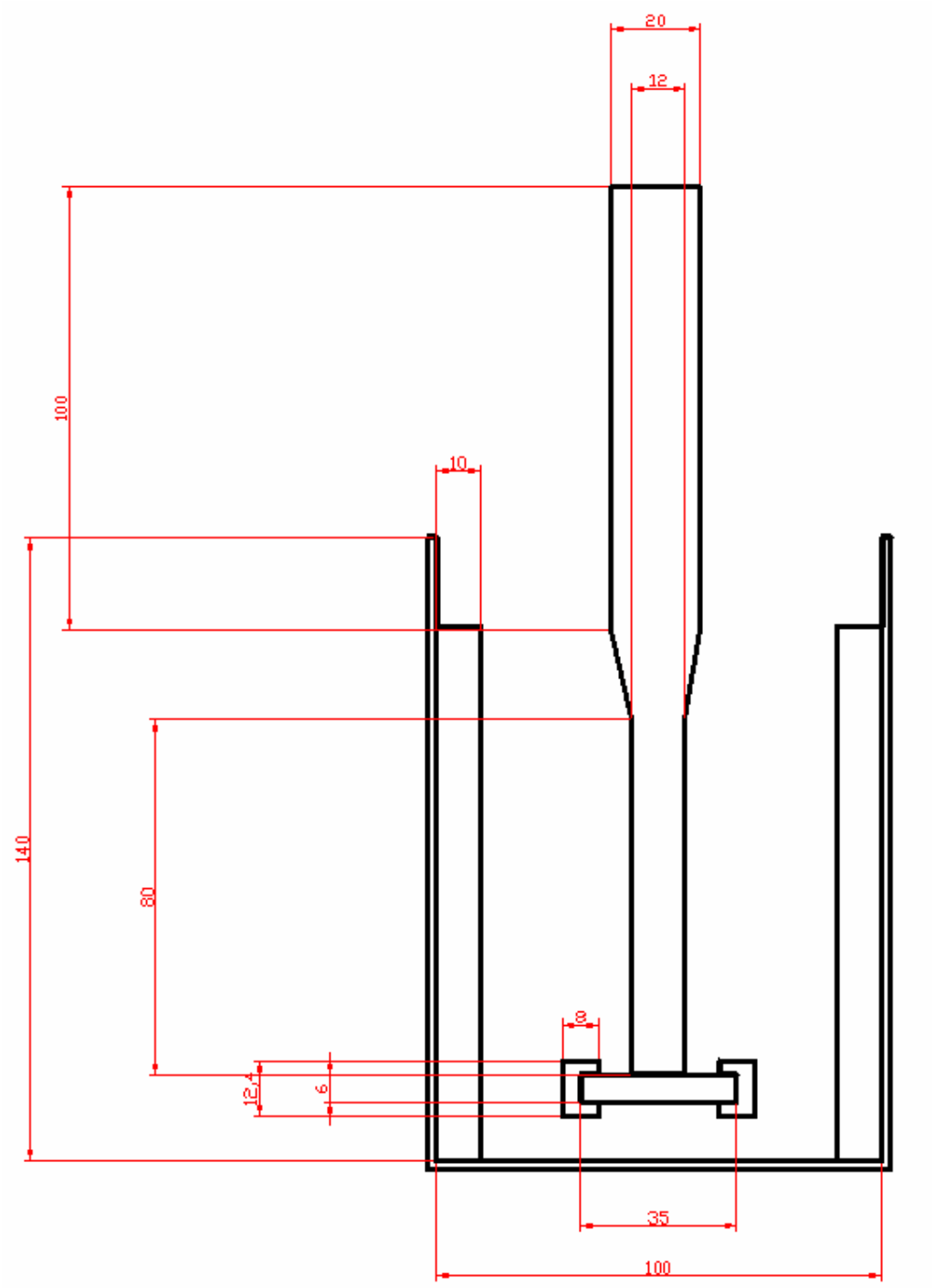

Fig A4.1: Design specifications of standard 4-blade Rushton impeller. The specified units are in mm

Appendix 5: List of chemicals

Number	Chemical name, molecular formulae	MW (g/mol)	Catalog number, Batch number	Supplier	Grade
1	Chloroauric acid, $HAuCl_4.3H_2O$	339.79	254169, 11315TD	Aldrich	99.999 %
2	Hydrazine hydrate, N_2H_5OH	50.06	38502, E05A-1005-1404-13	S.D. Fine Chem.	99 %
3	AOT, $C_{20}H_{37}O_7SNa$	444.55	D4422, 095K0203	Sigma	99 %
4	Brij 30, $C_{12}H_{25}(OCH_2CH_2)_4OH$	362.00	P4391, 093K01091	Sigma	98 %
5	Isooctane, C_8H_{18}	114.26	60471710001046, SL5SF51070	Merck	HPLC

Table A5. 1: List of chemicals used in this study for both preparing microemulsions and gold nanoparticles.